Design, Validation, Prototype Development of a Miniaturized, Compliant Torque Sensing System for use in Exoskeletons.

Author

FARYAL GULA

00000204637

Supervisor

DR. AMIR HAMZA

DEPARTMENT OF MECHATRONICS ENGINEERING

COLLEGE OF ELECTRICAL & MECHANICAL ENGINEERING

NATIONAL UNIVERSITY OF SCIENCES AND TECHNOLOGY

ISLAMABAD

AUGUST, 2021

Abstract

Exoskeletons for rehabilitation purposes are developed for use in physical therapy. Compliant torque sensors are needed in joints of Hand and Finger exoskeletons for accuracy and safe interaction. Spring-based series elastic actuation is popular for the soft mechanism of torque and force transfer between the exoskeleton and human fingers. Existing approaches for rehabilitation robotics use photo interrupters, encoders, magnetic encoders, optical encoders etc. having the complexity of assembly and increased size. In this research torque sensor is developed that accomplished the design requirements of stiffness, size, range, and linearity. The designs consist of an outer rim fixed and an inner rim to connect the moment arm for rotation. A single spiral link connects the fixed and the moving end of the sensor. Variation in the shape of the link is performed for better results. FEM Analysis is performed. Prototypes are implemented and validated.

Key Words: Torque, Sensor, Exoskeleton, Series elastic actuation

Table of Contents

List of Figures

List of Tables

CHAPTER 1: INTRODUCTION

In the United States, about 795000 Stroke patients appear annually [1]. In Pakistan, although the data is not available the situation is likely to be even worse. For the rehabilitation of stroke patients, wearable robots are used. In the design of these robots, sensors are used to measure torque, force, position and trajectory of joints. Accurate torque sensing is the basic requirement of all physical human-robot interactions. There are techniques to mitigate these errors and inaccuracies but to accomplish that task there is a need to measure these errors within a system. For this purpose, sensors are installed at locations vulnerable to errors. Such is the case with rehabilitation exoskeletons where a machine is physically directly interacting with a human body part. The force, torque, and trajectory that are being given to the human should be very accurate because crossing a human's threshold of force application can have severe consequences. In Exoskeleton Design for rehabilitation of Human finger torque sensor is required that can measure the single-axis force applied in opposite directions. For human-machine interaction in rehabilitation, there is a dire need for low stiffness materials and soft robotics design. Exoskeletons fabricated using additive manufacturing techniques are very popular among researchers as there is an ease of fabrication and freedom of designing. Additive Manufacturing is cost-effective and convenient as compared to CNC Machining, Laser Cutting, and EDM wire cutting. Miniature torque sensors are used to measure forces and torques in an exoskeleton. The sensor is also not waterproof. In this thesis, research has been performed on a single piece miniaturized compliant element that can be used for safe human-machine interaction in hand and finger exoskeleton.

CHAPTER 2: LITERATURE REVIEW

Sensors are basic elements of the exoskeleton that play a vital role in the accurate operation of an exoskeleton. Torque sensors are used to measure the force acting on a device. The majority of torque sensors have an elastic element that undergoes physical changes under the action of applied torque, which is being detected by a transducer and consequently, the transducer converts that physical quantity into an electrical quantity that is further processed by a controller. Using this methodology sensors are being designed. Strain gauges, encoders and Hall effect sensors are integrated by researchers into the sensor design.

Ubeda et al [2] designed a custom torque sensor for use in robot joints that measures torque on a single axis with a resolution of 0.002 Nm and sensitivity of 4.19 mV/Nm. Strain gauge is used as a transducer. The basic element of the design is a curved cross beam with a thickness of 6 mm incorporated in a structure having an overall diameter of 65 mm, mass 17.34 g, stiffness of 3.57x 10^6 Nm. AL-7075 is the material used for this design.

A dual-spiral-spring actuation system is developed for wearable robots to measure single-axis torque using two spiral springs in opposite directions as shown in Fig. 2.1 and an encoder is also installed. It has a thickness of 12 mm and a diameter of 90 mm. It can measure torque up to 2.4 Nm with a stiffness of 0.3 Nm/rad [3]. Spring steel is used for spiral spring.

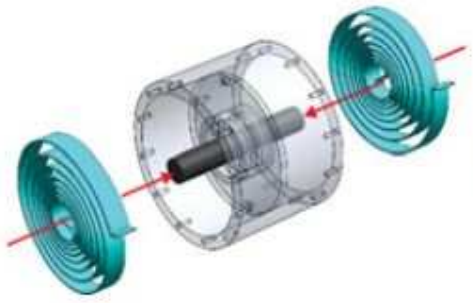

Figure 2.1: Complaint Joint Actuator Assembly [3]

Considering the high sensitivity requirements of a finger in a dexterous robot a single axis torque sensor of sensitivity 2.44 mV/V is designed. Using

strain gauges on beams as shown in Fig. 2.2, a 4-link structure symmetrical about x and y-axis is optimized to the size of 31mm x 4.2 mm measuring torque with a range of ±2Nm. The respective fabricated elastomer of AL7075-T6 achieved full-scale linearity of 0.62 %[4].

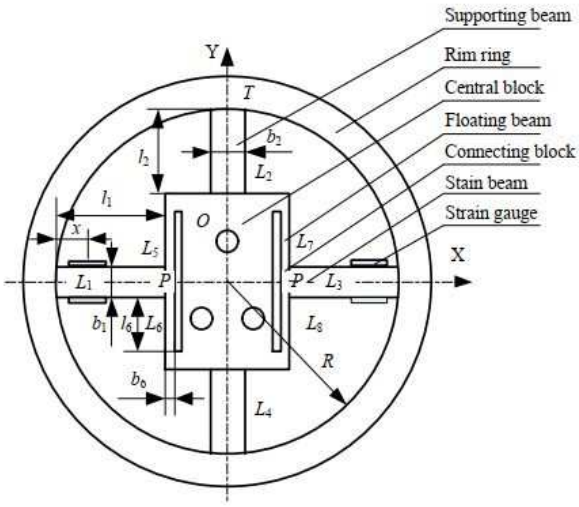

Figure 2.2: A single-axis torque sensor for dexterous robot [4]

For the safety of human-robot interaction to detect a collision, a sensor is designed that can measure torque on a single axis with a sensitivity of 33.49 mV/Nm and resolution 0.1 Nm design [5]. Strain gauges are attached on the links as shown in Fig. 2.3 in the holed structure of overall size ø78mm x 10mm with mass 75g and a capacity of 30Nm. The sensor is fabricated out of 7075 Aluminium alloy.

Figure 2.3: 4 link force/torque sensor of AL7075-T6 [5]

Torque sensor for knee and wrist joint is designed and the strain produced is verified analytically using Hooke's law, bending equation and Euler beam theory in comparison with FEA. The model measures force/moment in 6 axes using strain gauges on 4 beams made of aluminium confined in a ring of diameter 85mm for wrist and 120mm for the knee. However, experimental verification has not been done. The proposed material is aluminium [6].

Khan et al [7] had implemented a square cut torque sensor inside the hip joints of miniaturized hydraulically actuated quadruped robot-Mini HyQ. The author had achieved a high degree of linearity, symmetry, high sensitivity, scalability in terms of size and measurement range. This study suggested convenience in attaching and positioning strain gauges. The Square cut torque sensor design had two twin wings that are stretched or compressed depending on the torque clockwise/ counter-clockwise rotation only in a single axis. The overall diameter of the structure is 40mm, thickness is 15mm. The analytical model was verified experimentally.

Norman et al [8] presented seven prototypes of force-torque sensors based on optical photo interrupters for different applications. The sensors proposed are stiffer than strain gauge-based sensors. As the material used for 3d printing FFF technique is not homogenous therefore the mathematical models are quite complex and conventional formulae cannot be used but FEM Analysis can be employed for investigating different features of a design. However, Euler-Bernoulli beam theory can be used.

According to a comparison study [9], strain gauge based devices have the advantage of high scalability over encoder based torque/force sensors but they are more affected by temperature. Two torque sensor designs were evaluated for their merits and demerits in terms of cost, weight,

bandwidth, linearity error, crosstalk, ripple sensing time, thermal drift, resolution, noise, scalability, torque capacity, overload, safety factor and stiffness. Strain based design diameter of 63mm weighed 230 g with made of 17-4PH Steel. The other design having a magnetic encoder had a mass of 170 g and a diameter of 75mm made of Beta titanium Alloy SB20. Both target to

measure joint torque on a single axis of a robot with a maximum range of 150 Nm. However, strain-based design is stiffer (43450 Nm/rad) than encoder-based design (4507 Nm/rad). The design consists of 4 links and a symmetrical structure about the x and y-axis.

In a hexapod walking robot, ALPHA Peter et al [10] implemented a 3 axis F/T sensor that is better suited for three-axis measurements rather than five-axis. It uses a single torsion full-bridge strain gauge in combination with an onboard data processing as shown in Fig. 2.4. Installation and calibration have been simplified using pre-assembled PCBs. The authors have implemented mechanical compensation instead of conventional error reduction techniques. The sensor is low cost, compact and hermetically sealed having an overall diameter of 24.20 mm and height of 42.50 mm including the housing and accessories with a mass of 20g. Its force measurement range is 75N and for torque it is 1Nm. The sensor elastomer is made of AL6061-T6.

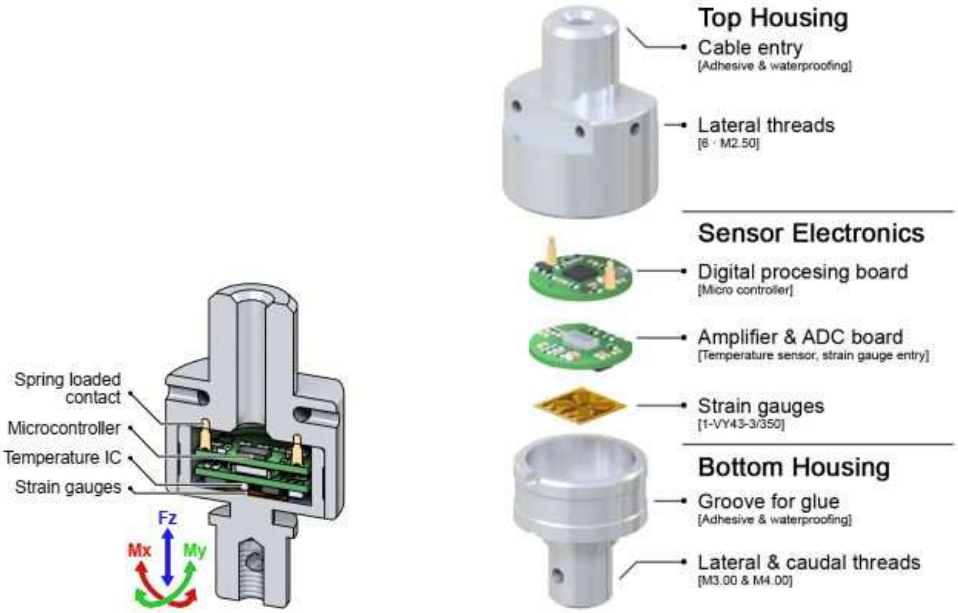

Figure 2.4 (a) Cross-section of the sensor **(b)** Exploded view of sensor assembly [10]

An elastic structure designed for 6 axes F/T measurement. Strain gauges are installed as shown in Fig. 2.5. The design consists of four T-shaped members that connect upper and lower parts for the effective detection of surface strains.

The T shaped beam further consists of an H-beam of thickness 1.6 mm and a V beam of 1.8 mm thickness. The sensor can measure various forces up to 200N and moments up to 10Nm [11]. Aluminium alloy has been machined to form the structure of elastomer.

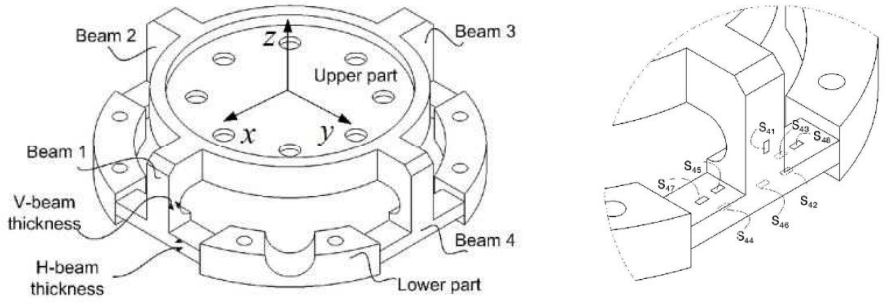

Figure 2.5 (a) Elastic Structure **(b)** Strain gauge locations [11]

A F/T sensor is integrated into a surgical shaft for use in minimally invasive surgery for measurement of Fz, Fy, Fx, Mx, My and Mz as shown in Fig. 2.6. Resolutions of the sensor are 0.08 N in radial directions, 0.25 N in the axial direction, and 2.4 Nmm in rotational directions and exhibit good linearity. Strain gauges are attached on 6 links that make up a flexural-hinged Stewart Platform of an overall diameter of 10 mm. Forces up to 30N and torques up to 0.3Nm can be measured. The structure is composed of AL7075 Aluminium alloy. Parameterized optimization method balances the sensitivity and stiffness of the flexible structure so as the range is also maximized [12].

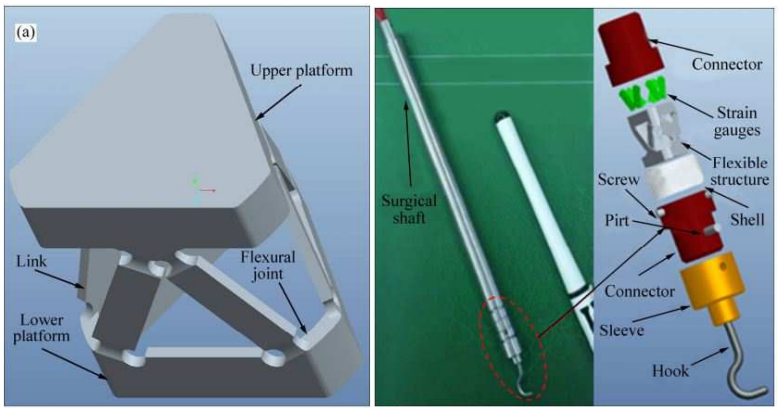

Figure 2.6 Six axis force/torque sensor for minimally invasive surgery [12].

Miniaturization results in a high degree of hysteresis, nonlinearity, and various design issues [13]. A commercially available photo-interrupter has been

used in a tendon-driven robotic hand to measure a force on a single axis at a maximum up to 200N with 1.85 % nonlinearity. The force sensor has been optimized to the size of 4 mm x 6 mm x 10 mm. The sensor assembly consists of a photo-interrupter, an elastic frame of AISI 4340 steel, and a PCB as shown in Fig. 2.7. The resolution of the sensor is 0.1N and the stiffness of the structure is 47.762 Nm/rad.

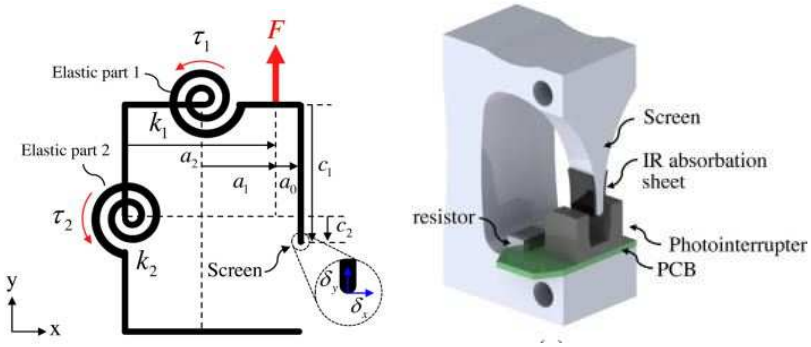

Figure 2.7 (a) Elastic structure realized as torsional springs **(b)** Sensor assembly [13]

For biomimetic robot joint, a single axis sensor of sensitivity is 2.06V/Nm is designed [14]. Photo interrupters are installed in a way that the interrupter shield is attached to the rib while the bracket is attached to the outer ring. The flexure spring structure consists of inner and outer flange connected by 2 ribs used as an elastic element for torque sensor as shown in Fig. 2.8. The overall diameter of the sensor is 60 mm while thickness is 4mm, mass is 16g and factor of safety is 4.5. The torque sensor offer measurement up to 1Nm on a single axis. The linearity of the sensor is 4.36% and the stiffness of the structure is 200Nm/rad. The material used is 7075 aluminium alloy.

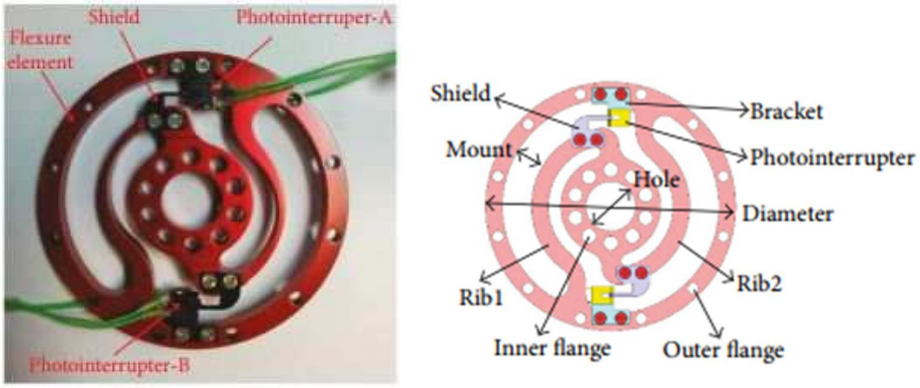

Figure 2.8 Single-axis torque sensor with photo-interrupters [14]

To investigate the aerodynamic force on a micro flapping wing of aerial vehicles a multi-axis sensor with a resolution of 003Nmm and sensitivity of 1.5V/N mm is achieved in [15]. U shaped and M shaped piezo resistors that work similarly to strain gauge are being used on T shaped links as shown in Fig. 2.9 for stress-strain measurement in response to the force or moment applied. This MEMs based sensor has dimensions of 11 mm x 11mm x 0.5mm and it is lighter than 0.1 g. The measurement range for Fx, Fy and Fz is 0-16N while for Mx and My is 0-15Nmm. The sensor offers linearity greater than 0.98.

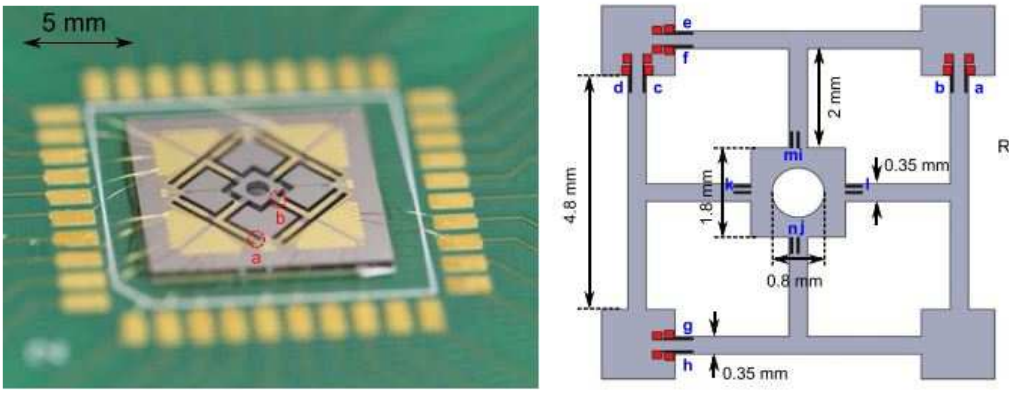

Figure 2.9 (a) Photograph of sensor prototype and the structures of piezo resistor marked with the red dash line circles **(b)** Dimensions of the sensor the piezo resistors are listed from a to n

The sensor [16] for robotic applications can measure torque on a single axis with a sensitivity of less than 0.01Nm.

The sensing principle is based on the variation of the photocurrent flowing through a Photodetector (PD) as a consequence of the variation of its relative position, with respect of a Light Emitting Diode (LED), caused by the deformation of the sensor frame under the effect of the torque to be measured [16]. The elastomer structure of overall size ø62 mm x 20 mm consists of an inner frame outer frame and three links as shown in Fig. 2.10. The sensor can measure torque on a single axis up to 2.4 Nm. The structure has a stiffness of 44Nm/ rad and ABS material is used.

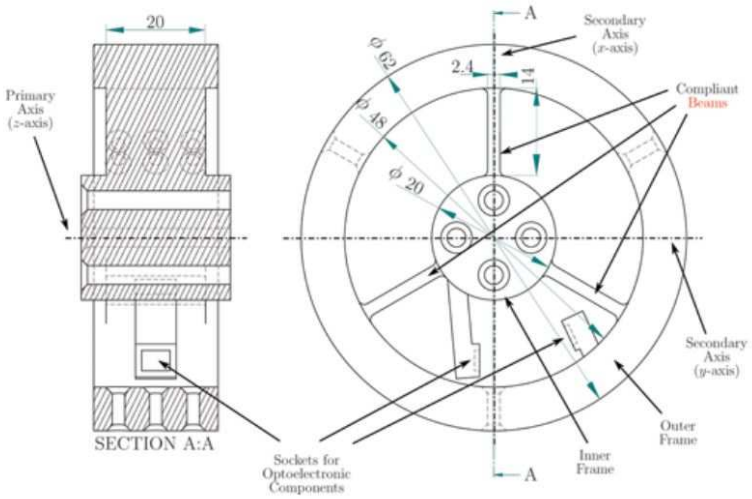

Figure 2.10: 3 link torque sensor design employing photodetectors [16].

For the applications requiring different measuring ranges and resolutions in robot joints, the torque sensor can provide variable resolutions of 0.0002948 Nm and 0.0016272 Nm in the small and large ranges of [0, 0.19 Nm] and [0.19 Nm, 2.3 Nm], respectively [17]. The torque applied on the flexure centre is measured by gauging the strains of radial flexures. The sensor is constructed by multiple radial flexures with different stiffness in series as shown in Fig. 2.11. The diameter of the structure is 68 mm and the thickness is 10 mm. The stiffness of the sensor is variable but for a small range, stiffness is 5.62 Nm/rad. The material used is Al7075-T6.

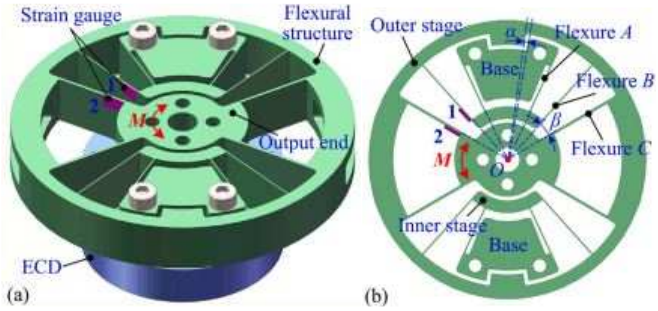

Figure 2.11: Variable stiffness torque sensor [17].

For various robotic applications, a 6 axis force-torque sensor is designed [18]. A comparison of AL2024 and PEEK has been done to demonstrate the pros and cons. The strain sensitivity of torque around the z-axis is 0.038 x10^{-}

^{4}/Nmm for PEEK and 0.00295 x 10^{-4}/Nmm for the aluminium alloy with a nonlinearity error of less than 1 %. Strain gauges are installed on a cross beam structure used as an elastic element. The dimensions of the sensor are 64 mm x 64 mm x 3.8 mm. The PEEK structure has a force measurement range of 30N and torque measurement range of ± 0.3Nm in x and y-axis ±0.5Nm in z-direction while the metallic structure has a range of 200N and torque range of ±2Nm in x and y direction ±4Nm in the z-direction. Because of its lightweight and high sensitivity, the PEEK sensor is very suitable for aerospace and medical fields, but PEEK is more sensitive to temperature than aluminium alloy.

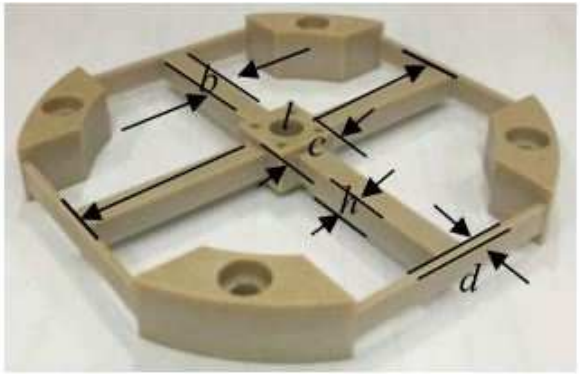

Figure 2.12: 4 link torque sensor design from Poly-etheretherketone [18]

The sensor is designed for wrist force sensing of robots [19]. 6 axis sensing is accomplished by the strain gauges are pasted on the flat surfaces of holes for maximum sensitivity of forces and torques. The structure consists of 4 radial beams and 4 circumferential beams and a central platform. The floating beams are converted to the H-beams as shown in Fig. 2.13 to improve the dynamic performance of the sensor and punching holes in beams and using parallel beams structures to increase the sensitivity of the sensor. The overall dimensions of the 6-axis force/torque sensor are Ø76 mm x 7 mm. The maximum force measurement range is 50N while for torque is 2.5 Nm. The material used is LY12 aluminium alloy.

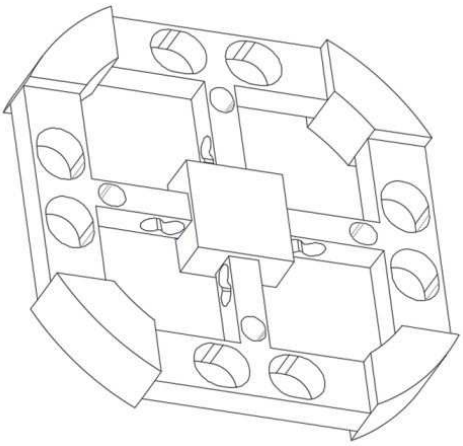

Figure 2.13: Wrist force sensor

For multi DOF robotic applications, a novel six-axis force-torque sensor with a resolution of 0.516 Nm is designed [20]. It works on the principle of capacitive sensing for detecting shear displacement change where two capacitive sensing parts and flour flexure hinges are used. Capacitance to voltage converter is used for signal processing. The design consists of 3 plate-shaped parts. Electrodes are placed at vertical locations and placed at both sides of PCB connected by hole as shown in Fig. 2.14. The dimensions of the sensor are ø 102 mm x 20 mm and the mass is 850 g. The maximum torque measured with this device is ±350 Nm.

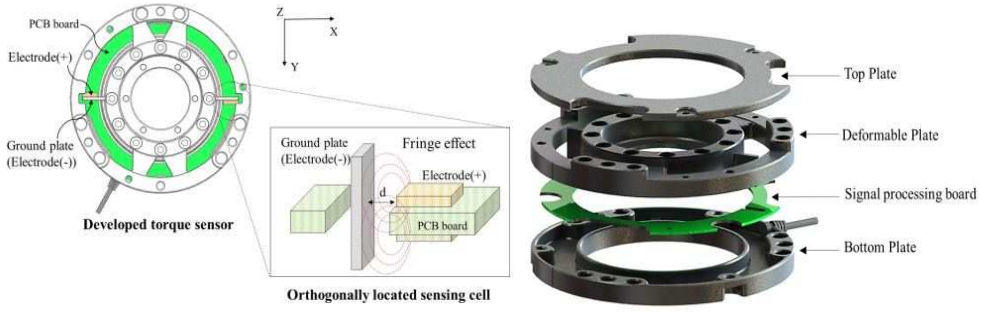

Figure 2.14: Capacitive torque sensor [20]

Torque sensors are affected by non-axial forces therefore [21] have high sensitivity for the one driving torque of interest, and yet very low sensitivity for the other five force/torque components.

Table 2.1 summarizes the parameters of the torque sensors designed by researchers for robotic application. A variety of transducers have been incorporated into the force-torque sensing systems which act as a defining factor of the design process.

Table 2.1: Review table of torque sensors

Paper	Transducer	Diameter (mm)	Material	No of axes Measurement	Year
Zhang et al [27].	Piezo resistor	11 x 11 x 0.5	Silicon	5	2016
Kim et al [3].	Encoder	90	spring steel	single	2013
Liu et al[14].	Photo interrupter	60	AL7075	single	2018
Yong et al[28].	Fiber Bragg Grating	26	Aluminium alloy	3 axis	2009
Kim et al[8].	Encoder	65	AL7075	–	2018
Kim et al [20].	Capacitance to digital converter	102	–	6 axis	2016
Norman et al[8].	Photo interrupters	-	PLA	6	2020
Seok Hwan Jeong[13].	Photointerrupers	4 x 6 x 10	AISI 4340 Steel	single	2018
Palli and Pirozzi[16].	Photodetector	62	ABS	Single	2014
Kashiri et al [9].	Encoder	74	Beta-Titanium alloy (SB20)	single	2017

Table 2.2 shows that mostly aluminium alloys are being picked by researchers for the elastomer of torque sensors that incorporate strain gauge as the transducer. Aluminium alloys that have more impurities exhibit better properties in terms of strength and elasticity.

Table 2.2: Review table of Strain gauge-based torque sensors

Paper	Diameter	Material	No of axis measurement	Year	Torque Range	Stiffness	Application
Ubeda et al [2]	65mm	AL7075-T6	single	2018	1Nm	3.57x10^6	Industrial robotic
Khan et al [7]	40mm	Steel alloy	single	2017	60Nm	31.3Nm/rad	Robot Mini-Hyq
Li Kun et al [12]	10mm	AL7075	6	2015	0.3Nm	High	Minimally invasive
Hu et al [19]	76mm	LY12-Al	6	2018	3Nm	-	Robot
Han et al [4]	34mm	AL7075-T6	Single	2019	2Nm	High	Dexterous robot
Fu et al [18]	64mm	PEEK	6	2019	0.5Nm	NA	Industrial robot wrist
Zhang et al [15]	75mm	AL6061-T6	6	2016	40Nm	19512Nm/rad	Industrial robot
Lou et al [5]	78mm	AL7075	single	2019	30Nm	NA	light-weighted
Ma et al [29]	68mm	2AL12	6	2013	12Nm	NA	Robotic Manipulator
Kashiri et al [9]	63mm	17-4PH	single	2017	150Nm	43450Nm/rad	
Sun etal [17]	68 mm	AL7075-T6	single	2021	2.3 Nm	5.62 Nm/rad	Robot Joint
Aghili et al [21]	95mm	steel	6	2014	300Nm	2.4 x10^5$	direct-drive motor in
Our Design	30mm	PLA	single axis	2021	0.5Nm	1.4Nm/rad	Exoskeletons and

2.1 Material

Choice of material depends upon the application for which the sensor is being required. As for industrial robots' material with high elastic modulus and strength is preferred. For applications where there is close interaction between human and robot-like exoskeletons and prostheses, there is a need for soft material with less resistance to deformation/displacement. Researchers have used aluminium alloys for this sensor. Aluminium alloys are lighter than steel alloys. They are easily available in the market at a low cost. Aluminium has a lesser elastic modulus than Steel alloys while greater strength than Composite materials. Elastic modulus is the measure of resistance provided by the material to deformation. Steel has an elastic modulus of 210 GPa which is much higher than aluminium alloys i.e., 70 GPa on average. Therefore, aluminium alloys would produce more strain in response to the torque/force applied. Fig. 2.15, Fig. 2.16, and table 2.3 suggest aluminium as the best choice for the complaint sensor design as it is stronger than polymers but less stiff than steel alloys. From the literature, it is quite clear that designers have used aluminium alloys for sensor elastomers in strain-based designs.

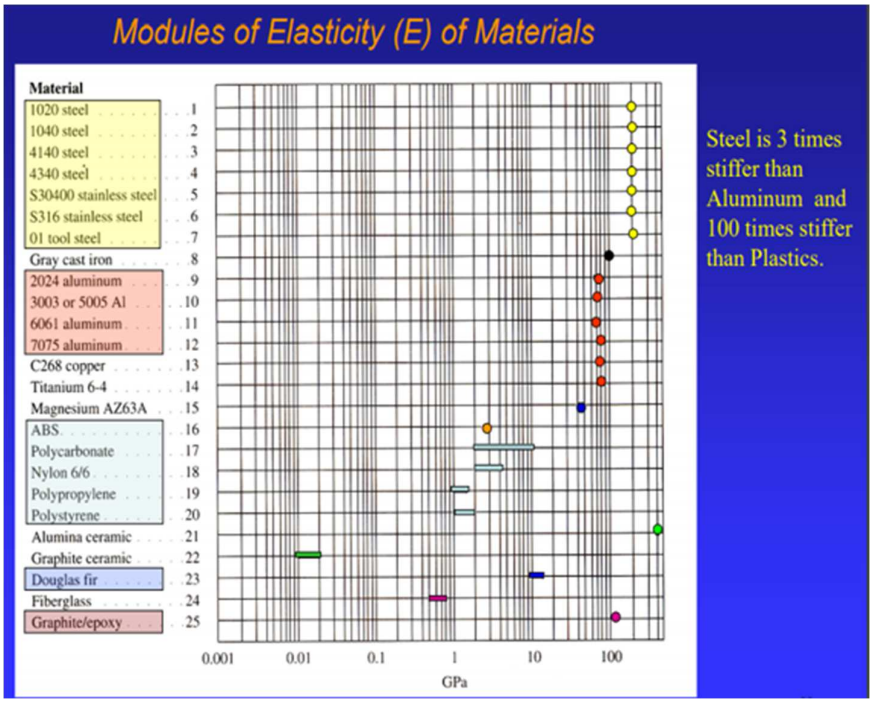

Figure 2.15: Comparison of materials concerning Elasticity

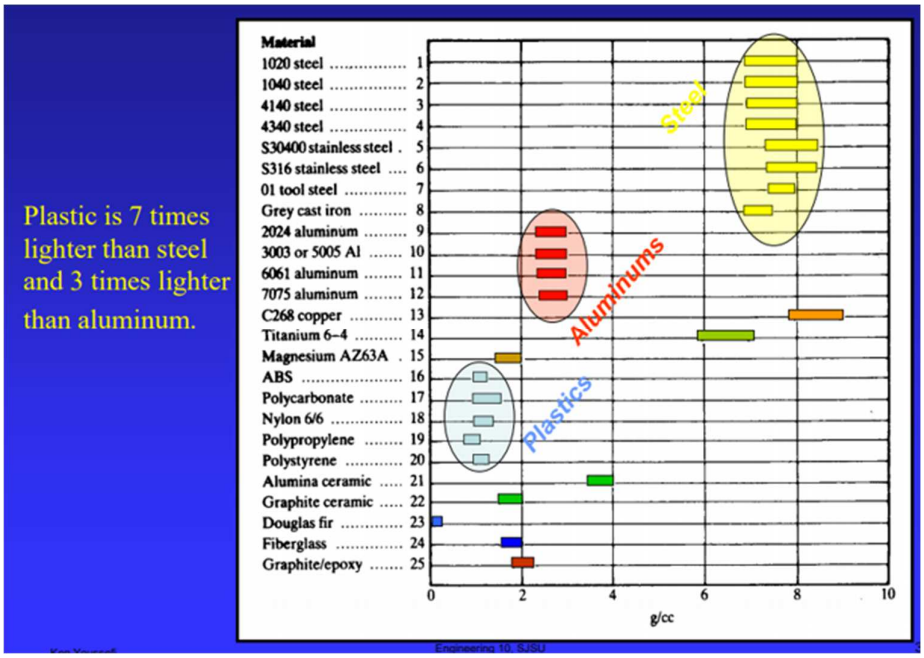

Figure 2.16: Comparison of materials with respect to density

According to the table 2.1 the Al6061-T6 and Al7075-T6 among aluminium alloys have better compatibility for use in torque sensors for exoskeletons. Among polymers PEEK has a good tensile yield strength for use in sensor design.

Table 2.3: Properties of generally used materials

Alloy	Elastic Modulus	Tensile Yield Strength	Density	Machineability
Al 7075-T6 [22]	71.7 GPa	503 MPa	2.81 g/cc	70 %
Structural Steel	210 GPa	630 MPa	7.85 g/cc	
Al 6063-T6 [23]	68.9 GPa	214 MPa	2.7 g/cc	50 %
Al 6061-T6 [23]	68.9 GPa	276 MPa	2.7 g/cc	60 %
Al 2024-T6 [24]	72.4 GPa	345 MPa	2.78 g/cc	70 %
PLA [25]	3.5 GPa	65.7 MPa	1.25×10^{-9} g/cc	
ABS [26]	2.9 GPa	27.6 MPa	1.21 mg/m^3	
PEEK [18]	4.2 GPa	70 MPa	1.3 mg/m^3	

Table 2.4 provides a comparison between state-of-the-art strain gauges. The most important feature in a strain gauge is the gauge factor that is representative of sensitivity. Metal-based strain gauges have much lower sensitivity than semiconductor-based strain gauges. But there is a trade-off between sensitivity and temperature effects.

Table 2.4: Review of Commercially available Strain gauges

Strain Gauge	Gauge Factor	Nominal Resistance	Size (mm)
KFH-6-120-C1-11 L1M2R [30]	2	120	4.5x3.9 to 25.2 x4.8
KFH-6-350-C1-11 L1M2R [30]	2	350	4.5x3.9 to 25.2 x4.8
DY43-3/350 [31]	2	350	8.2 x 8
SS-250-225-120PB [32]	100	120	3.29 x 76.2
KFG-02-120-C1-23 L1M2R [33]	2.25	119.6	3.3x2.4

2.2 Design Requirements

In robots design, scientists have focused on joints to have sensors for torque, force, position, and trajectory control. Size of the sensor is mostly relative to the size of the robot and location of sensors i.e., in prosthesis or exoskeletons if the sensor is to be utilized in finger joints, then 31mm diameter is the lowest size achieved [4]. According to a survey [34] by Cukurova University, Turkey the width of the DIP joint of the index finger ranges from 13.69 mm to 16.22 mm while the PIP joint lies at 16.20 mm to 19.01mm that motivated by the thickness/width of the sensor to be 10mm at most. According to rehabilitation experiments [35] by Ueki et al, the torque required for index finger PIP and DIP joints are 0.29Nm therefore the maximum range of the torque sensor is set 0.5Nm so that the strength of the elastomer is not compromised. In [36] stiffness is as low as 1.985 Nm/rad with an objective of 1.6Nm/rad. The sensors that include strain gauge as primary transducer have the main aim of linearity because stress cannot be applied more than the elastomer's elastic limit else the material will get plastically deformed. Linearity of strain is also desired to simplify and optimize the calibration else curve fitting technique can also be utilized for nonlinear results.

Table 2.5: Design requirements for torque sensors in finger exoskeletons

Parameters	**Goals**
Diameter	30 mm
Width	18 mm
Max Torque	0.3 Nm
Mass	Mass of exo/5
Stiffness	1.6 Nm/rad
Linearity of strain	Yes
Readily integrable with existing prosthesis/exoskeleton designs	Yes
Easily machineable using local resources	Yes
Optimized Design	Yes

CHAPTER 3: DESIGN AND SIMULATIONS

Various designs of torque sensors according to the requirements have been implemented. There is always a static part of the design which is fixed or grounded and apart from which force or torque is exerted. In exoskeletons for cable-driven design, it is important to have a circular design i.e., a design having an outer rim to attach cables and exert force to the next part. For applications where there is a force/torque transmission between links then a polygon design i.e., square or rectangle can also be used. According to the application outer or inner rim, both can be selected for the fixed and moveable end. However, both have displacement with respect to each other so based on the scenario moveable and fixed ends can be exchanged. Therefore, the fixed and moveable ends are circular in the proposed design. The links connecting the outer and inner rim can be classified as beams. Overall parameters of the design are affected by beam design, length, thickness, type, and number.

3.1 Initial Design

The design of the elastomer starts with a circular rim of diameter 30 mm according to the design requirement and an inner rim of 5 mm. Commonly available strain gauges have a size of 4.1 mm x 7 mm hence the thickness is kept at 5 mm at least. According to Euler beam theory

$$\delta = \frac{\mathrm{M}}{\mathrm{EI}}$$

$$I = \frac{bh^3}{12}$$

$$\delta = \mathrm{R}\,\Delta\theta$$

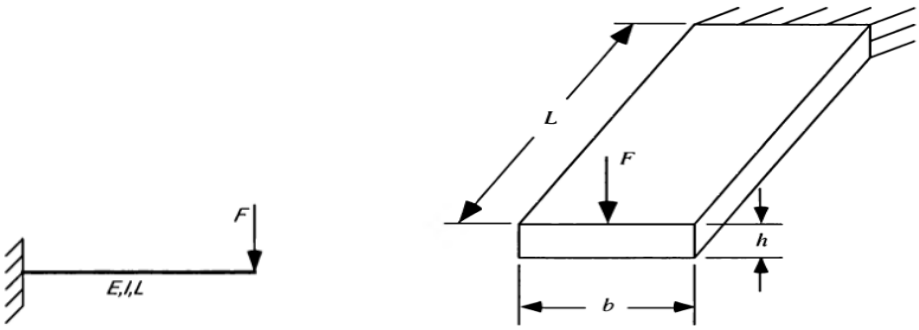

Figure 3.1 Cantilever beam with known force or load

where δ is deflection, M is the moment applied, E is the elastic modulus of the material, I is the mass moment of inertia, R is the radius of the outer rim and Δθ.

3.1.1 4 Link Design

The outer and inner rims are connected by 4 beams as shown in Fig. 3.2. According to the ANSYS simulation of this design, the stiffness is much greater than the objective.

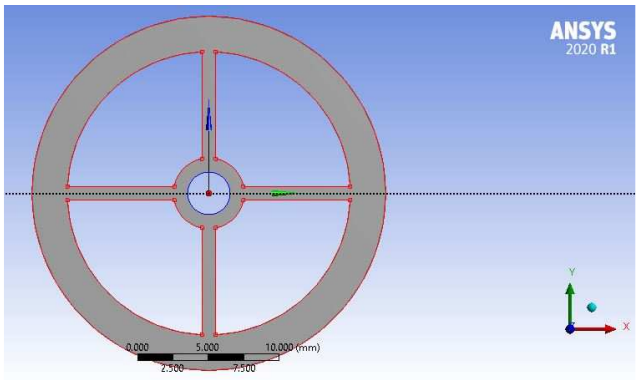

Figure 3.2: Four link design

Table 3.1: Parameters of 4-link torque sensor design.

Dimension/ Parameter	Value
Link width	1mm
Link length	7.54mm
No of Links	4
overall diameter	25mm
Thickness	5mm
stiffness	142 Nm/rad

3.1.2 3-Link Design

According to Euler beam theory the stiffness of structure can be reduced by increasing beam length. Therefore, the shape of beam is made zig-zag to increase length and the number of beams are reduced.

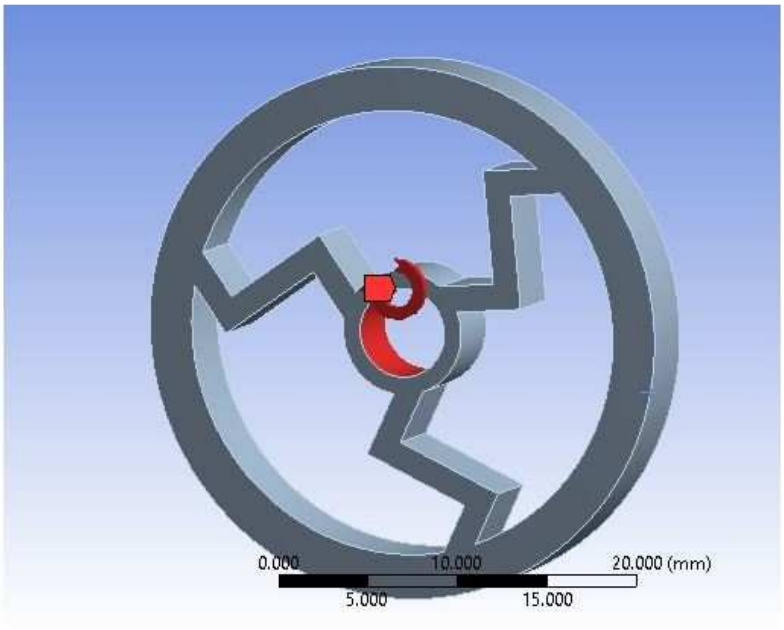

Figure 3.3: 3-link design

Table 3.2: Parameters of 3-link design

Dimension/Parameter	Value
Link width	1mm
Link length	10.97 mm
No of Links	3
overall diameter	30mm
Thickness	5mm
Stiffness (PLA)	5.8Nm/rad
Stiffness (AL7075-T6)	109.2Nm/rad
Stiffness (AL6061-T6)	105 Nm/rad

3.1.3 2-link design

To decrease stiffness number of beams are reduced to two. To increase the length the shape of the beam is changed to curve and in this way, stiffness is reduced but the goal is still not achieved.

Further the number of links are decreased to two to meet stiffness requirement. Beam is changed to a more regular Archimedean curve shape. Width and thickness also reduced. The

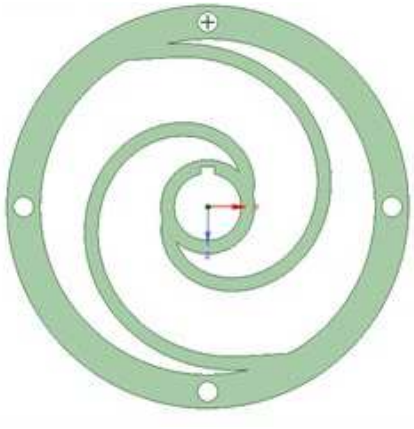

Figure 3.4: 2-link design

Table 3.3: Parameters of 2-link design

Dimension/Parameter	**Value**
Link width	1mm
Link length	31.8mm
No of Links	2
overall diameter	30mm
Thickness	5mm
Stiffness	6.1 Nm/rad

In Fig. 3.5 the axis was displaced from its centre which would impose issues in operation and inaccuracies in measurement. The linear deformation would add to the resultant strain due to rotation.

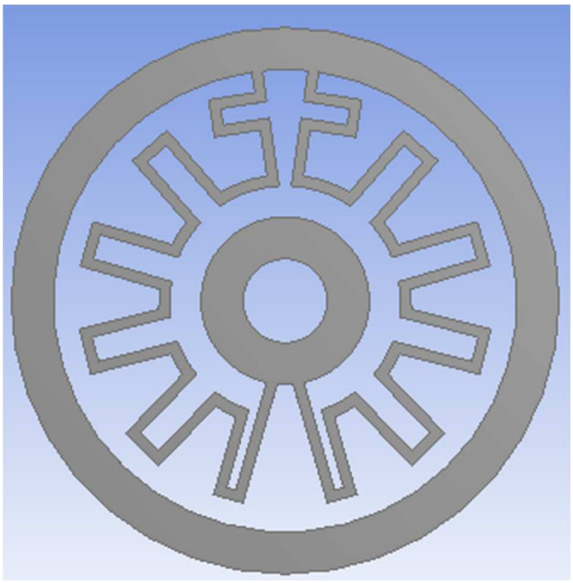

Figure 3.5: 2-link design having increased length

3.2 Spiral link design

A single beam is designed in a spiral shape that increases the length but decreases the stiffness to our desired parameter. According to Euler Beam Theory, the relationship between beam stiffness and beam design in a spiral structure [3] is

$$Ks = \frac{Etw^3}{12L}$$

$$\delta = \mathrm{R}\,\Delta\theta$$

$$\mathrm{Ss} = \frac{6\mathrm{M}}{\mathrm{tw}^2}$$

E is Elastic Modulus, M is moment applied, Ks is the stiffness, L is the length of the beam, t is the thickness of the beam, w is the width of the beam, Ss is the stress on beam. According to Euler Beam Theory the relationship between beam stiffness and beam design in a spiral structure

$$\delta = \frac{Fl^3}{3EI}$$

$$k = \frac{3EI}{l^3}$$

E is Elastic Modulus, M is moment applied, Ks is the stiffness, L is the length of the beam, t is the thickness of the beam, w is the width of the beam, Ss is the stress on beam.

According to the equation, the decrease in width of beam and increase in length of the beam decreases stiffness. The tensile yield strength of AL6061-T6 is 276 MPa. The stress on the design should not exceed 276 MPa at maximum torque. For a design to bear a torque of 0.3 Nm safety factor should be greater than 1. In this way, the stress to strain relation would also be linear that shows the structure is performing under its elastic limit. Although the FEM analysis structure would not break, plastic deformation would occur and eventually, the sensor would become inaccurate.

3.3 FEM Analysis

After thorough literature and simulations over different scenarios in ANSYS six designs are proposed for prototype development.

A moment of 300 Nmm is applied in the centre rim and an equivalent von mises P stress of 270 MPa is produced. i.e., at the corners in the link. All designs have the same outer diameter of 30 mm, the link width of the outer rim is 2.5 mm and thickness of 5 mm. The inner rim has a rectangle key. The material is AL6061-T6. A single beam is designed in a spiral shape that increases the length but decreases the stiffness to our desired parameter.

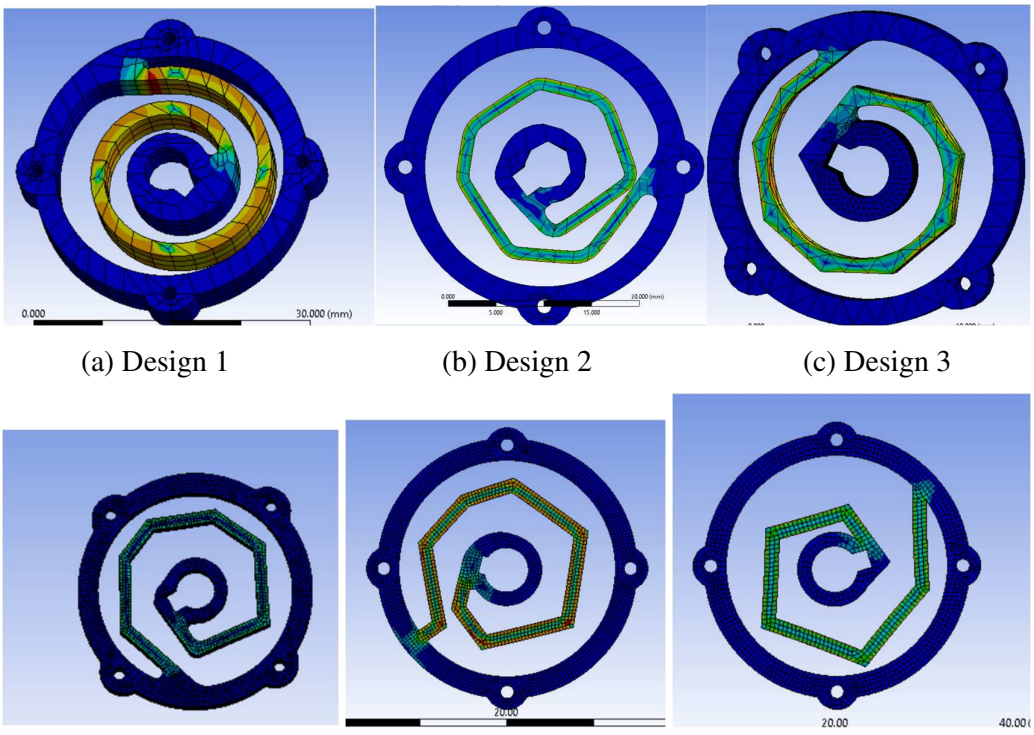

(a) Design 1 (b) Design 2 (c) Design 3

(d) Design 4 (e) Design 5 (f) Design 6

Figure 3.6: Proposed Designs

Table 3.4: Parameters of proposed designs

Designs	Link length	Link Width	Stiffness	Mass
Design 1	70.92 mm	1.5 mm	1.37 Nm/rad	6.2 g
Design 2	69.8071 mm	1.5 mm	1.33 Nm/rad	6.2 g
Design 3	56.35 mm	1mm to 1.67 mm	1.59 Nm/rad	6.5 g
Design 4	54.4 mm	1.4 mm	1.73 Nm/rad	4.8 g
Design 5	60 mm	1.5 mm	1.58 Nm/rad	5.1 g
Design 6	54.72 mm	1.5 mm	1.8 Nm/rad	NA

3.3.1 Design 1

Fig. 3.7 shows the safety factor result of simulation with the application of 300Nmm torque applied in the centre. The FEM results suggest that the structure will not break as the safety factor value is 1.06.

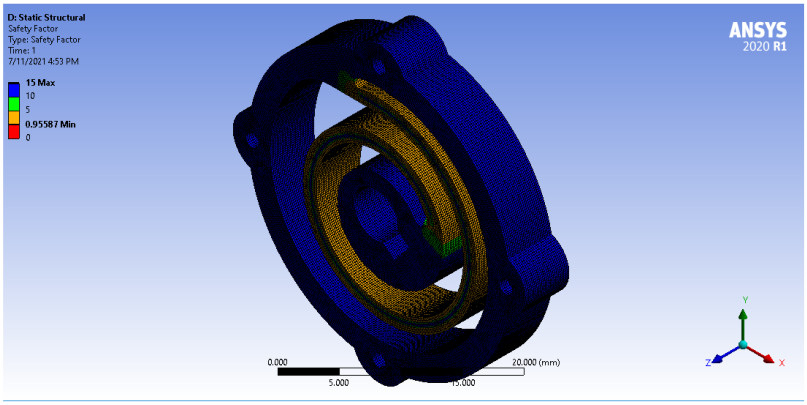

Figure 3.7: Safety factor of Design 1

Fig. 3.8 shows that the stress is under the safe range of tensile yield strength while the highest stress point is near the fixed end of the spiral link.

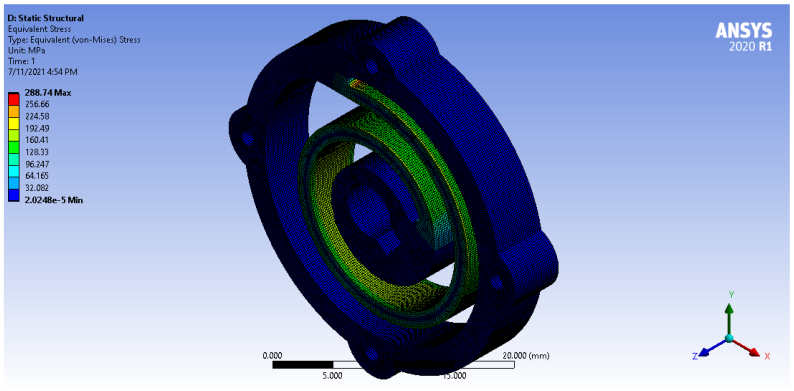

Figure 3.8: Equivalent von mises Stress Contour of Design 1

Rotation in response to the torque applied is measured by using a remote point in the centre of the elastomer and inserting the flexible rotation probe at that point to give the angular of rotation as shown in Fig. 3.9.

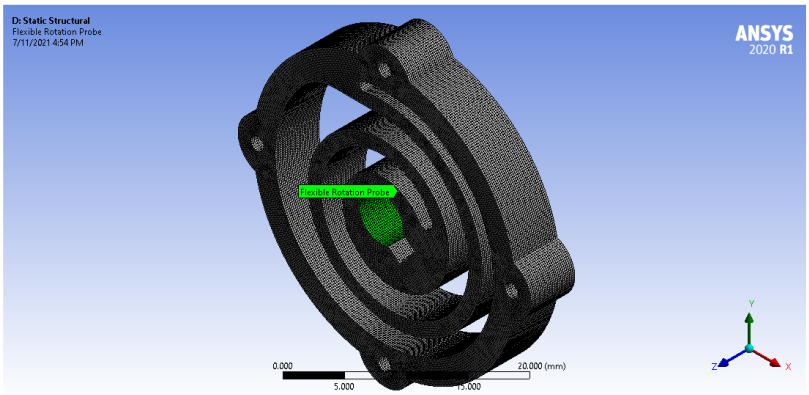

Figure 3.9: Location of rotation probe of Design 1

The distribution of strain in the spiral link is shown in Fig. 3.10 when 300 Nmm torque is applied. While strain probe is located on the desired location of the strain gauge as shown in Fig. 3.11. The strain probe analyses strain at a specific point.

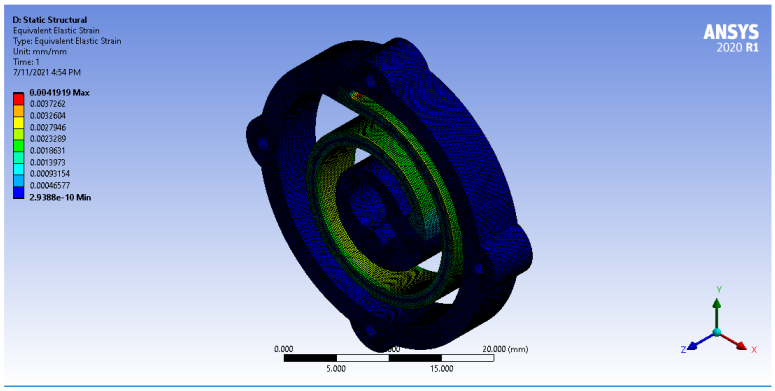

Figure 3.10: Equivalent von mises stress of Design 1

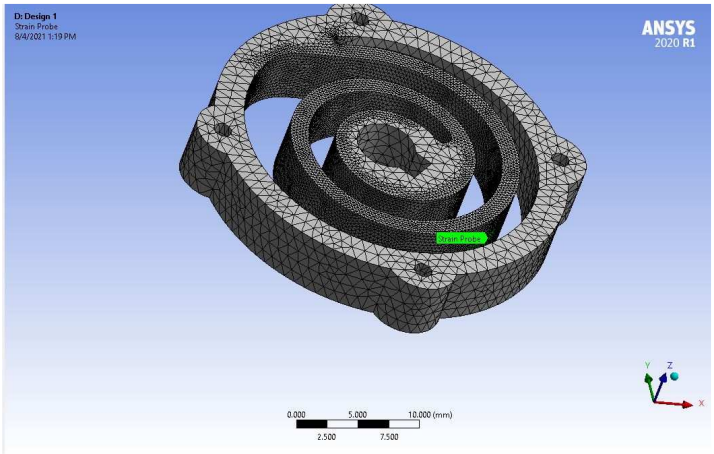

Figure 3.11: Location of strain probe on Design 1

3.3.2 Design 2

Fig. 3.12 shows that the structure will not distort by the application of maximum torque for the design. This fact is supported by Fig. 3.13 where the maximum stress observed in ANSYS simulation is 270.8 MPa which is less than the tensile yield strength.

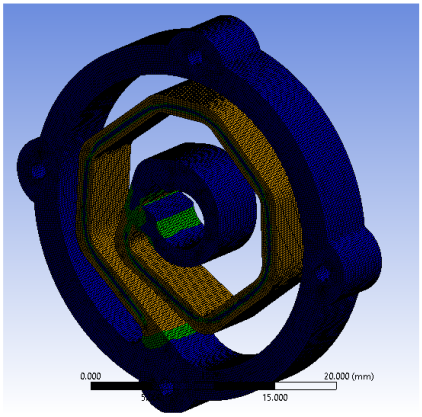

Figure 3.12: Safety factor of Design 2

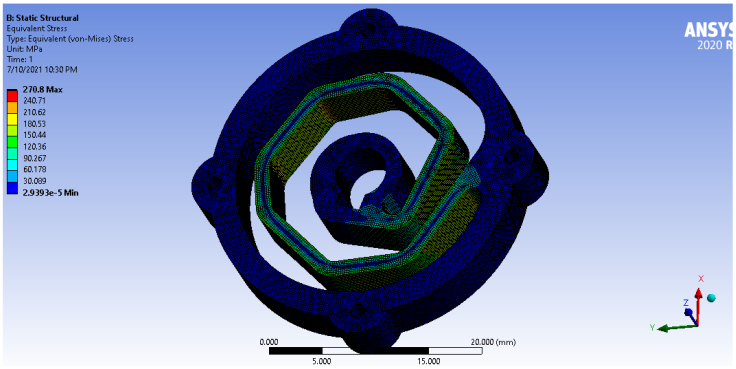

Figure 3.13: Equivalent von mises stress on Design 2

The desired location for strain gauge attachment is shown in Fig. 3.14 where a strain probe is inserted for better measurement of strain at that part of the link.

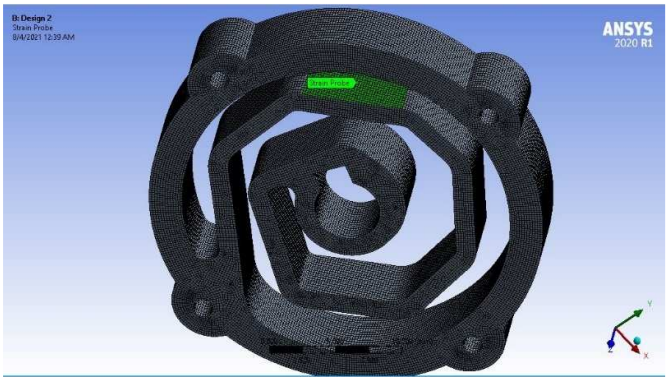

Figure 3.14: Strain probe location on Design 2

3.3.3 Design 3

Fig. 3.15 shows that the elastomer can give elastic deformation under the range of 300 Nmm torque.

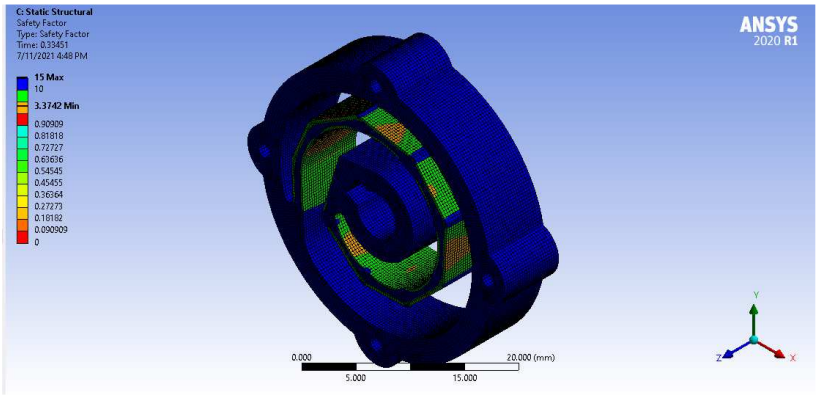

Figure 3.15: Safety Factor of Design 3

In Fig. 3.16 the maximum stress shown is 244 MPa that is lower than the tensile yield strength i.e., 276 MPa. This shows that this structure can work at torques greater than 300 Nmm.

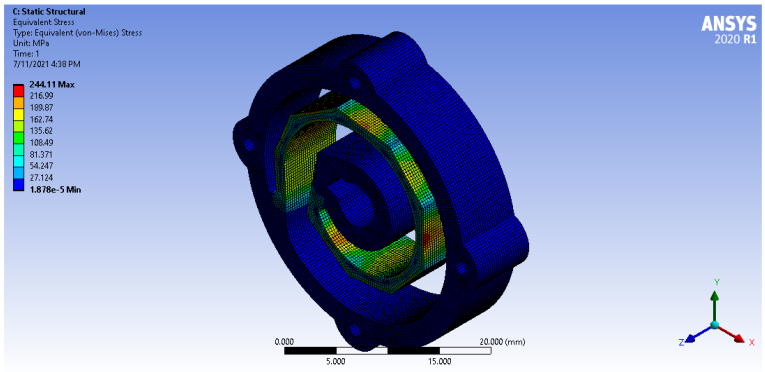

Figure 3.16: Equivalent von mises stress on Design 3

In Fig. 3.17 the equivalent elastic strain is greater in the centre of the flat-surfaced of the link i.e. 0.003543 mm/mm. The location of high strain is selected for strain gauge installation. In Fig. 3.18 the strain probe is used at the desired location for strain measurement.

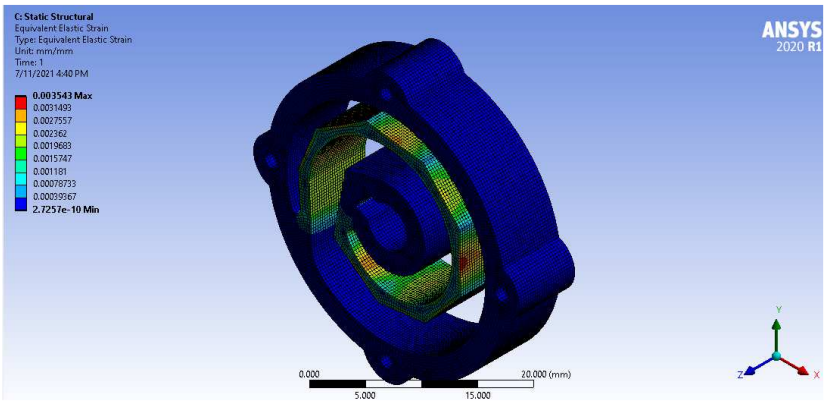

Figure 3.17: Equivalent von mises strain on Design 3

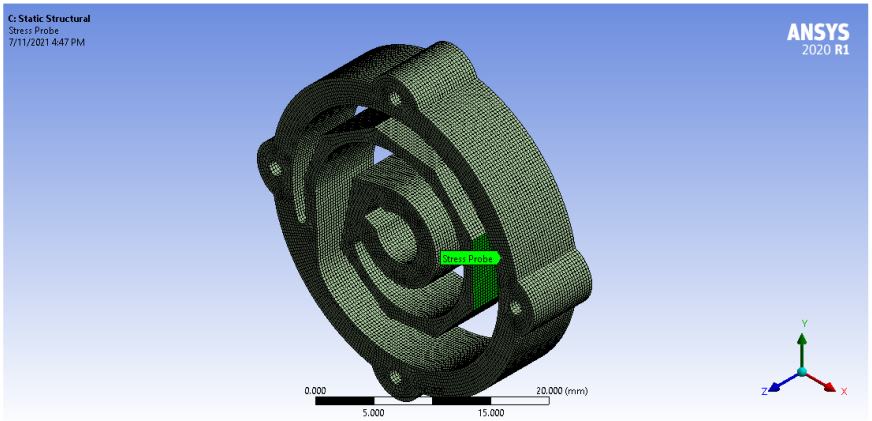

Figure 3.18: Strain Probe on Design 3

3.3.4 Design 4

In Fig. 3.19 the resulting maximum equivalent von mises stress is 328 MPa when 300 Nmm torque is applied, the stress concentrates at the corners in the link. There is a greater possibility of plastic deformation in the range of 0 to 300 Nmm.

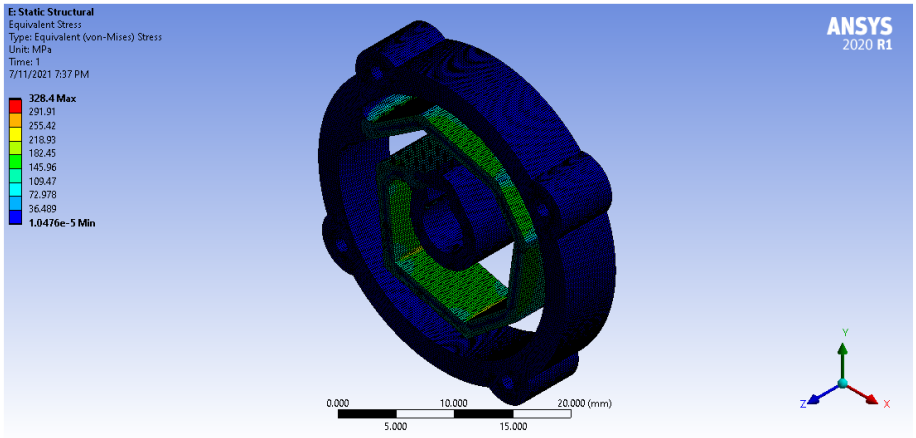

Figure 3.19: Equivalent von mises Stress on Design 4

The equivalent von mises strain from FEM Analysis is 0.0045 mm/mm shown in Fig. 3.20 predicts the elastomer to be more sensitive as compared to other designs.

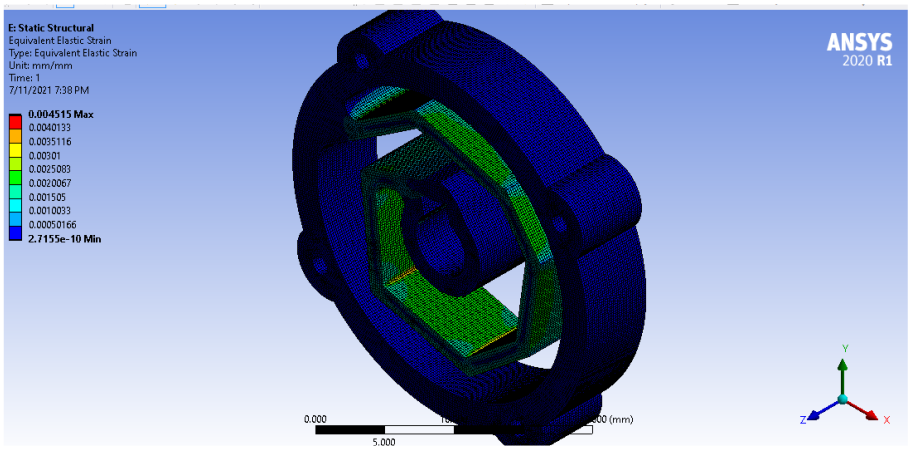

Figure 3.20: Equivalent von mises strain on Design 4

3.3.5 Design 5

In Fig. 3.21 it is evident that the von mises stress is greater than the yield strength of Al6061-T6 that poses a threat of plastic deformation at a maximum torque of 300 Nmm that is the requirement of the design.

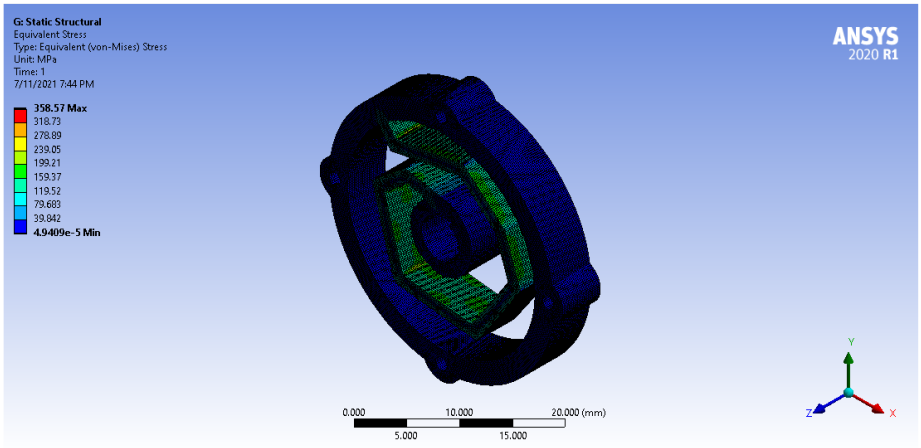

Figure 3.21: Equivalent von mises Stress on Design 5

Similarly, the maximum strain in FEM Analyses is 0.005229 is shown in Fig. 3.22. The maximum strain is concentrated at the corners in the link. This elastomer can provide high sensitivity and good resolution for torque sensing, but it cannot work up to the required maximum torque due to the danger of plastic deformation and fracture.

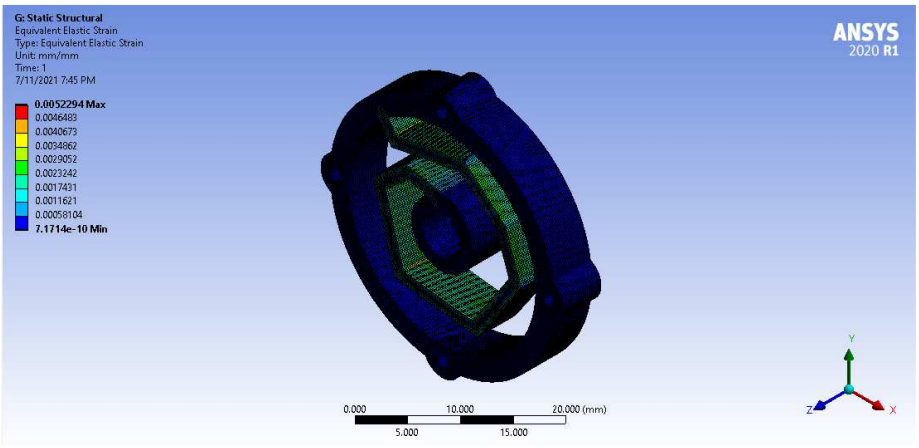

Figure 3.22: Equivalent von mises strain on Design 5

3.3.6 Design 6

This design is stiffer than all other designs proposed in this research, and it doesn't meet the design requirements. In Fig. 3.21 the maximum stress is 360 MPa and in Fig. 3.23 the maximum strain is 0.0052704.

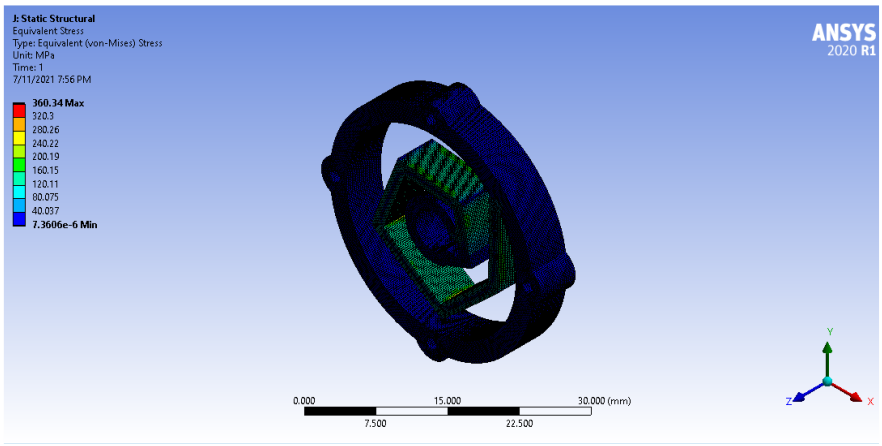

Figure 3.23: Equivalent von mises stress on Design 6

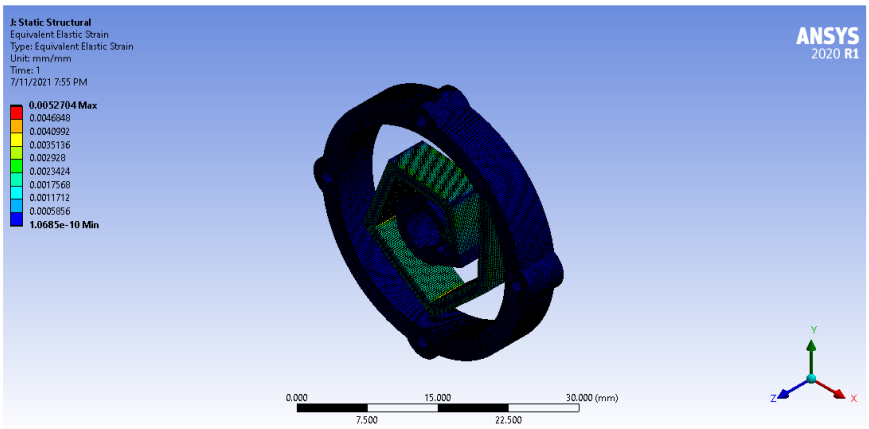

Figure 3.24: Equivalent von mises strain on Design 6

CHAPTER 4: EXPERIMENTAL SETUP

4.1 Fabrication

CNC Machining is less costly than EDM Wire cutting. For CNC Machining end mill required should not be more than 1 mm diameter as the profile has a narrow path. Therefore, EDM Wire cutting and laser cutting is preferred over CNC. Complex and narrow profiles can be cut through a metal sheet using wire cutting and laser cutting. Laser cutting has a limitation of sheet thickness due to the reflective surface of the Aluminum sheet. Therefore, wire cutting is done and the specimens are presented in Fig. 4.1. For a polymer structure, the 3D printer using additive manufacturing process is very convenient, fast and it can fabricate complex structures.

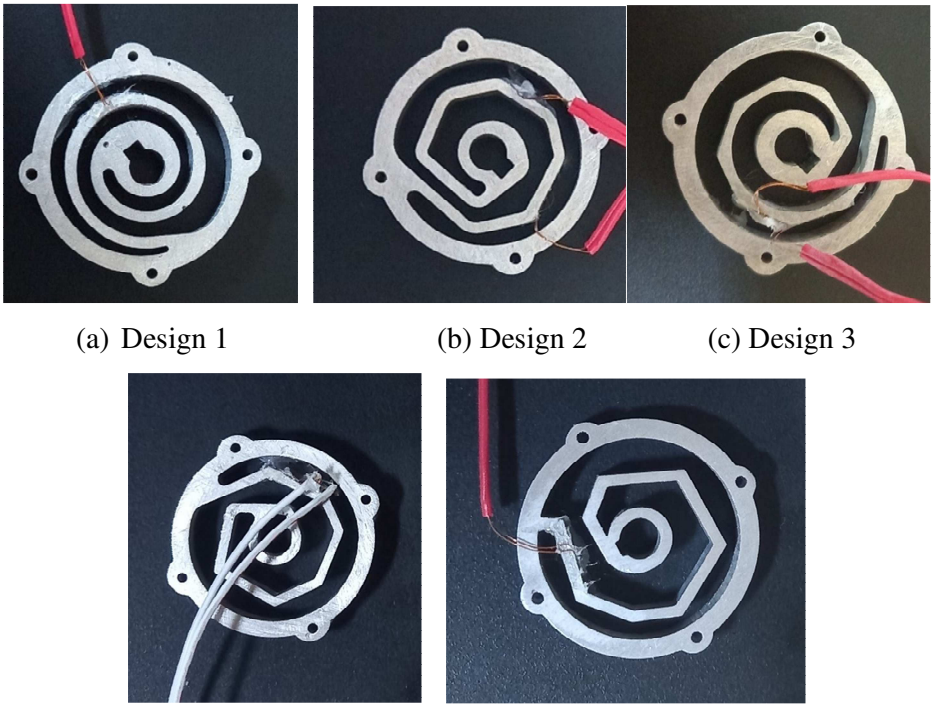

(a) Design 1 (b) Design 2 (c) Design 3

(d) Design 4 (e) Design 5

Figure 4.1: Wire Cut Elastomers of AL6061-T6

4.2 Strain Gauge

The strain gauge for this application has been procured from KYOWA TECHNOLOGIES JAPAN. As the material of elastomer is an aluminum alloy that is why a compatible strain gauge in terms of coefficient of thermal expansion is selected. The model of the strain gauge is KFGS-02-120-C1-23 L30C2R. It comes with pre-

attached wired so that the labour of soldering wires to pads in strain gauges is saved. The surface of the metal is cleaned with acetone and then using adhesive CC-33A that is 2 ethyl cyanoacrylate is used for strain gauge attachment. The gauge factor of this strain gauge is 2.27 and the resistance is 120 ohm.

4.3 Amplification Circuit

As the signal from the bridge circuit is very low requires the need to use a differential amplifier that can increase the potential from microvolts and millivolts to volts with a noise reduction. INA125P is an amplifier and HX711 is 24 bits analog to digital converter module that can be used for this purpose.

The strain gauge is incorporated in a traditional bridge circuit the differential voltage is then amplified using an instrumentation amplifier INA125P as shown in Fig. 4.2. The gain of INA125P depends inversely on the value of Rg [37]. As a result, the input potential is elevated by 3004 in the proposed circuit.

Hence the strain is converted to a change in resistance that is followed by respective variation in voltage which is amplified for the better recognition of measurements.

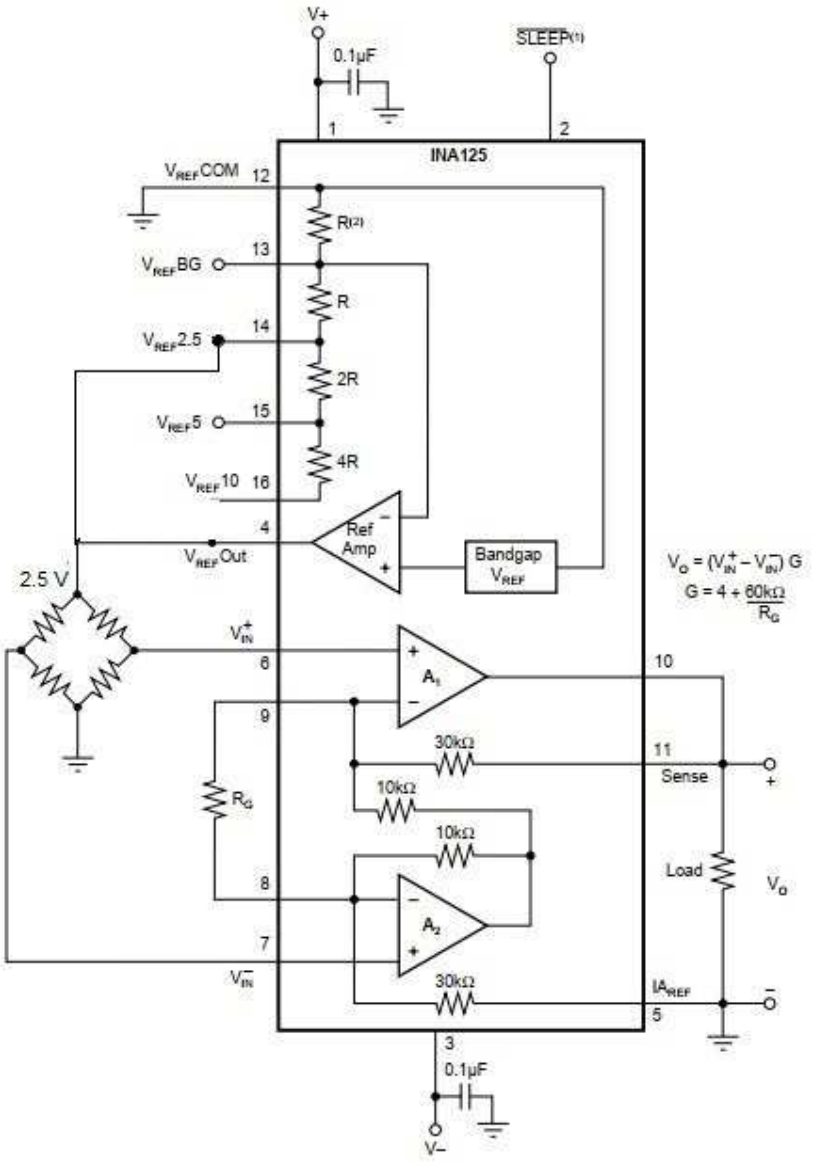

Figure 4.2: Amplification Circuit [37]

The circuit is first tested on a breadboard and then fabricated on PCB as shown in Fig. 4.3 using resistors of 1% tolerance so that changes in the environment doesn't induce errors.

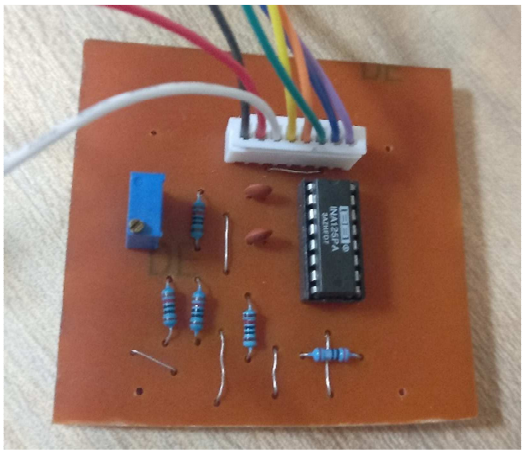

Figure 4.3: PCB circuit

4.4 Experimental setup

The experimental setup for the torque measurement and validation is demonstrated in Fig. 4.4. The weights are suspended using a hook via a moment arm of 5 cm length that transfers torque to the centre of the elastomer. The strain produced in the link is measured by a strain gauge using the amplifier. The resulting signal is acquired using NI MYRIO 1900 and the LabVIEW software.

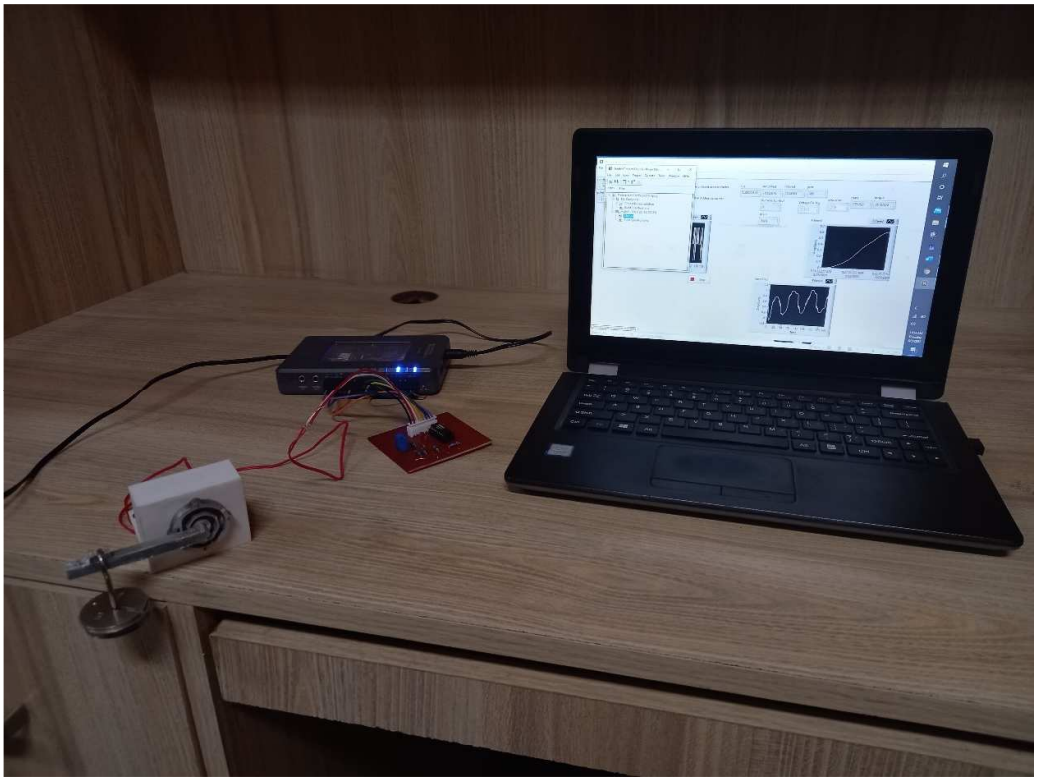

Figure 4.4: Experimental setup

CHAPTER 5: RESULTS

The torque sensor designs have merits and demerits that are predicted from ANSYS Simulations. Design 1 structure is strong enough for the torque range and stiffness, but it does not have a smooth surface for convenience in strain gauge installation. Design 2 and design 3 have the provision of smooth surfaces for strain gauge attachment. The stress does not exceed the tensile yield strength for the range of 0 to 300 Nmm and they exhibit more deformation than design 1 for detection of strain. That is why these two designs are selected for experimental study and torque-sensing application sin exoskeletons. Design 4 and Design 5 display a safety factor less than 1 for 300 Nmm torque which tells us about the infeasibility of the design in the required torque range. Design 6 has a stiffness greater than 1.6 Nm/rad consequently it is also not favourable for low stiff and soft robotic applications. Therefore, designs 2 and 3 have been selected for experiments and evaluations. They are experimentally tested, verified, and validated.

5.1 Design 2

The strain is measured using the amplified voltage readings of the sensor and the recorded readings are presented in Fig. 5.1 in the form of a graph. There is a variable error of 3% to 10 %.

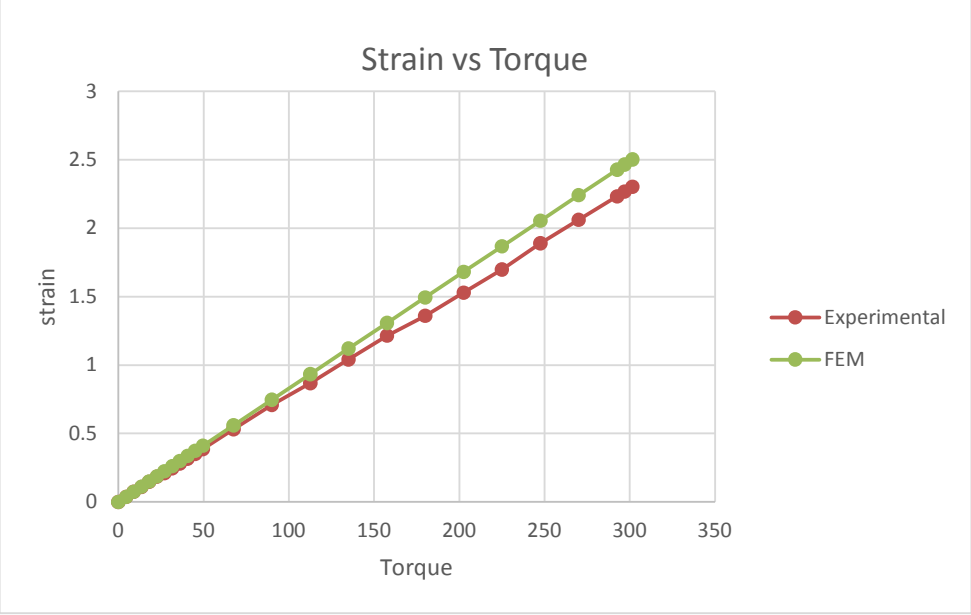

Figure 5.1 Comparison of strain measured experimentally with the FEM analysis

Fig. 5.2 presents the voltage results of the sensor corresponding to the torque applied. The sensor has a zero error of 0.2V and a maximum voltage of -8.76 V. The relation between torque and output voltage is linear that is it is convenient to calibrate.

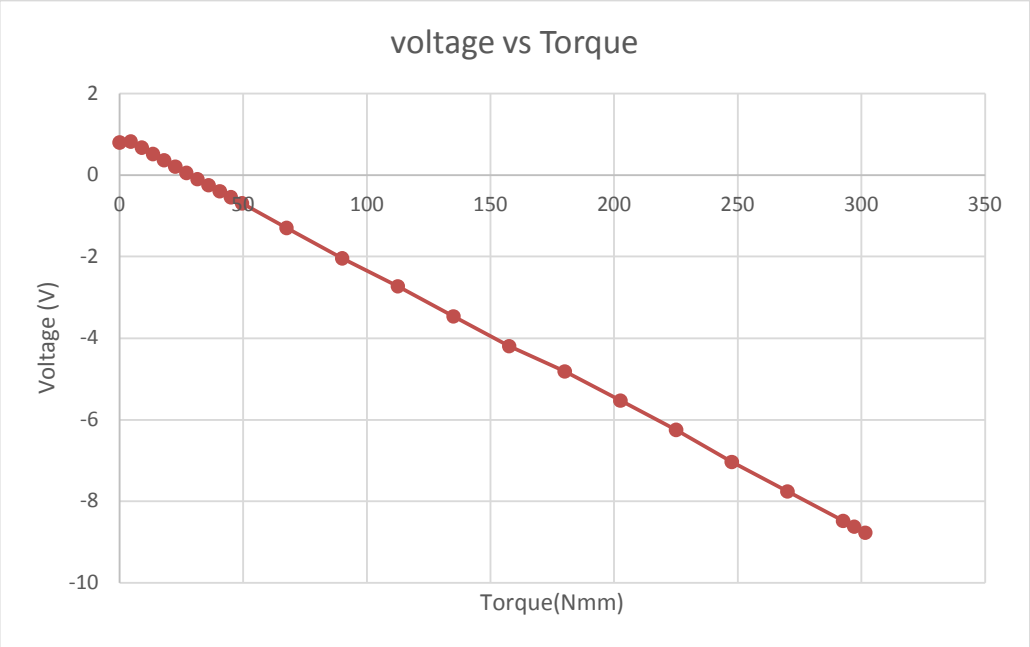

Figure 5.2: Measured voltage of the sensor in response to the torque applied

The graph in Fig. 5.3 is the FEM Result of the flexible rotation probe with respect to the torque applied. The relationship is linear and maximum rotation is 12.15 degrees. So, the range of motion of the sensor is 12.15 degrees.

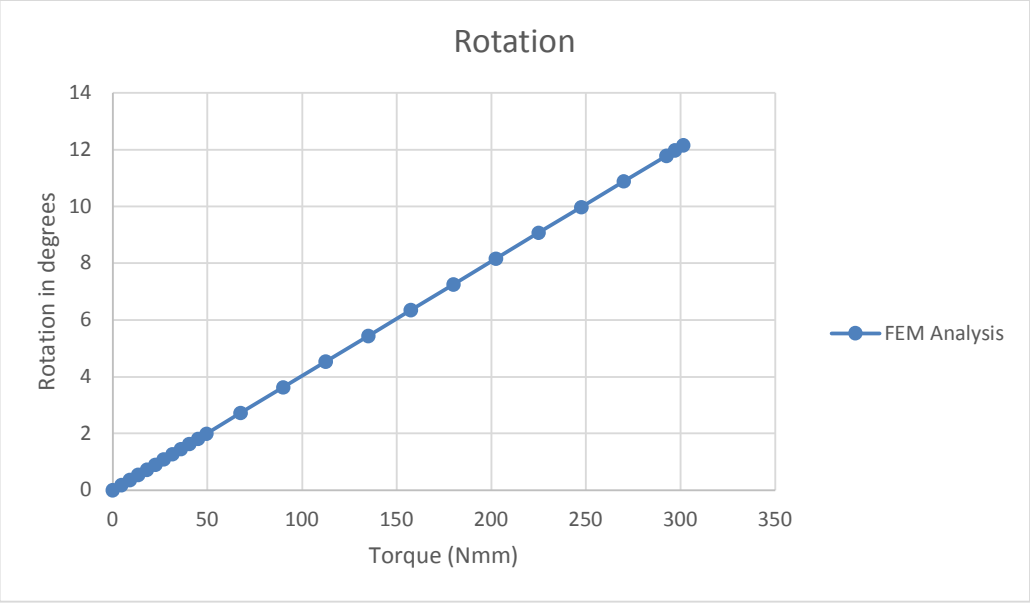

Figure 5.3: Rotation of the sensor with respect to the torque applied on Design 2

According to FEM analysis, the relationship between stress and torque in the range of 0 to 300 Nmm is linear as depicted in Fig. 5.4.

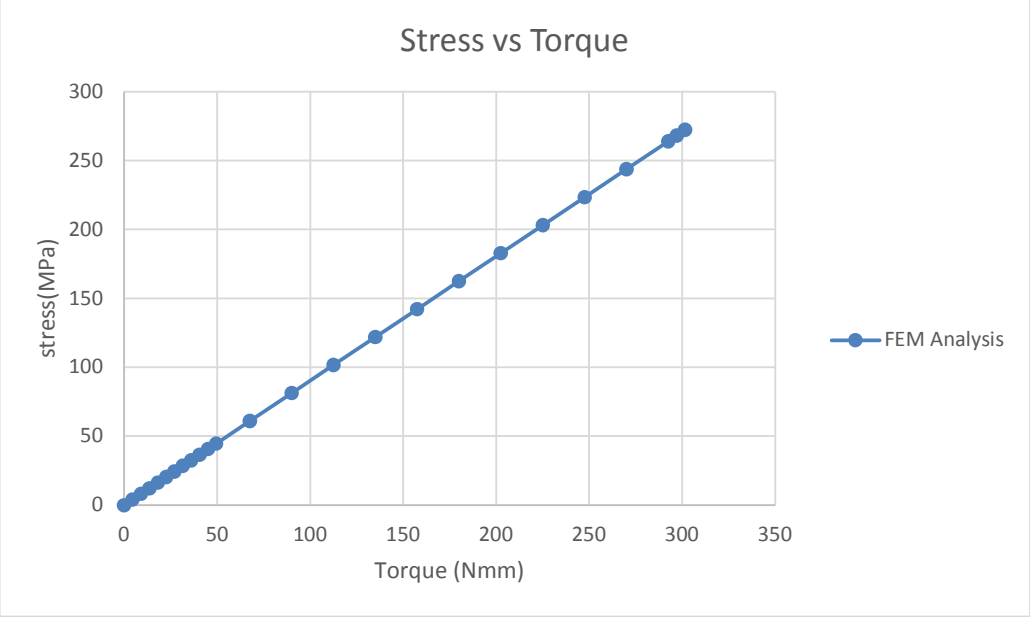

Figure 5.4: Equivalent von mises stress of Design 2

5.2 Design 3

The strain measured from strain gauge using amplifier and LabVIEW is recorded in a form of a graph in Fig. 5.5 and compared with the FEM strain. The relationship is linear; however, the experimental graph moves away from the FEM at torques near the upper limit of the sensor. The error is 2% to 11%.

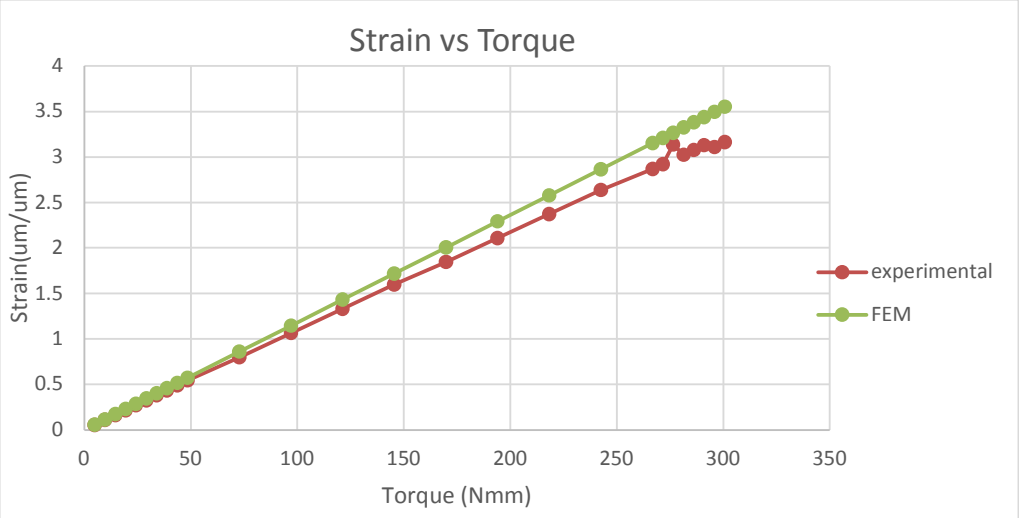

Figure 5.5 Comparison of strain measured experimentally with the FEM analysis

The voltage output of the sensor for the range of 0 to 300Nmm torque is presented in Fig. 5.6. The relationship is linear and the voltage ranges from 0.2 V to 14.5 V.

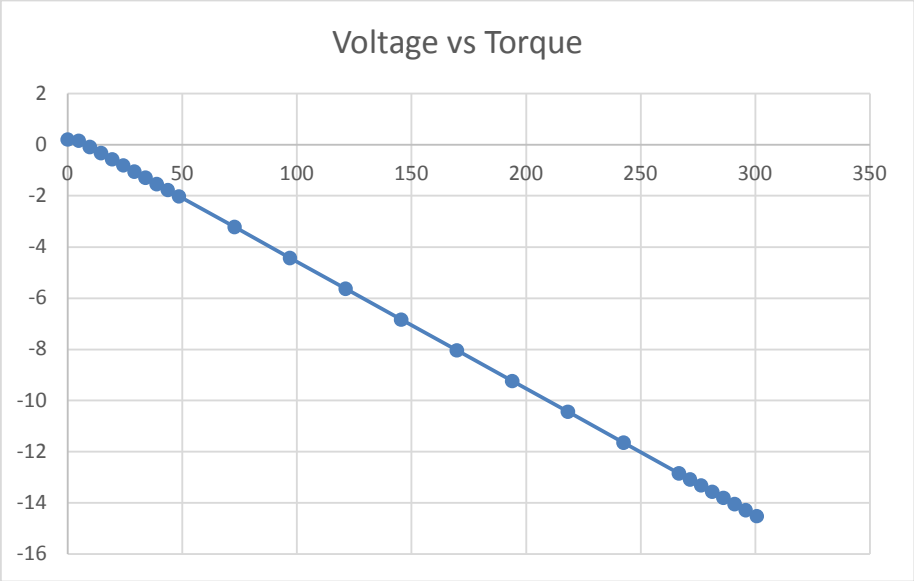

Figure 5.6: Output Voltage corresponding to applied Torque

The FEM Analysis of stress vs torque is depicted in Fig. 5.6. The relationship is linear until the stress reaches the tensile yield strength and at 360 Nmm the equivalent von mises stress is 294 MPa that leads the structure into plastic deformation.

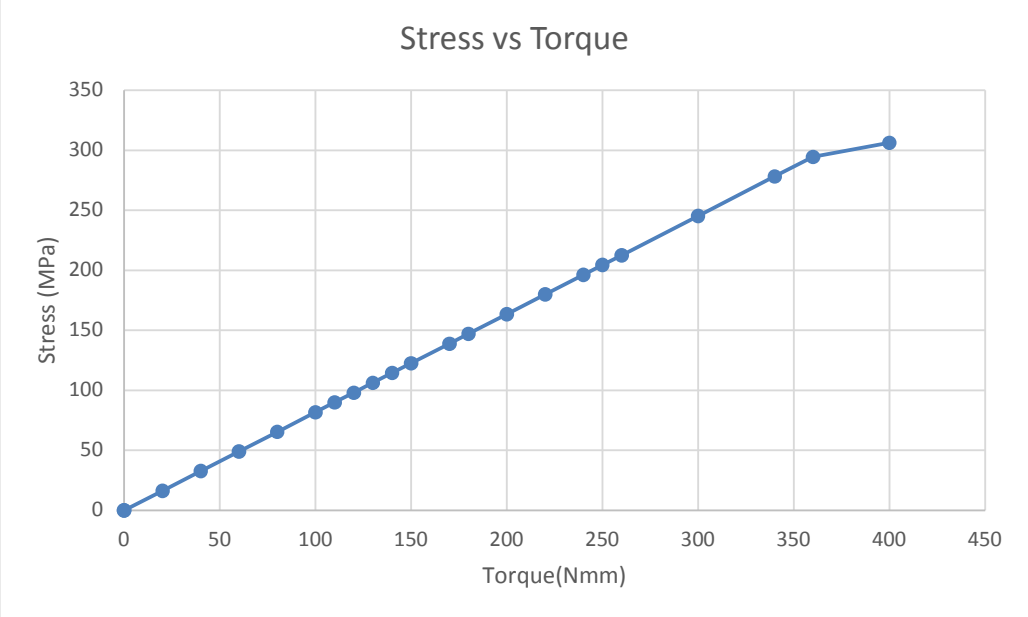

Figure 5.7: FEM Analysis of Stress to torque

CHAPTER 6: CONCLUSION

Exoskeletons for rehabilitation is a modern technology to facilitate stroke patients with physiotherapy. In finger exoskeletons, accurate torque sensing is the basic need for smooth operation and precise motion. Therefore, torque sensors are needed in finger exoskeletons that are less stiff, small in size, light in weight, sensitive to small torques with accuracy and with greater resolution. Researchers have implemented series elastic actuation using springs and encoders for accurate torque control. The torque sensor consists of an elastic element, transducer, and signal conditioning circuit. Torque sensors for exoskeletons have been designed using magnetic encoders, optical encoders, potentiometers, piezo resistors, photodetectors, photo interrupters etc. Strain gauge-based sensors can be miniaturized and scaled down to a greater extent than encoder-based force/torque sensors. Therefore, a strain gauge is selected as a transducer. AL6061-T6 is selected as the elastomer material. Linearity of output to input is also an advantage of strain gauge. The design of the elastomer consists of a single spiral link of thickness 1.5 mm. The outer diameter is 30 mm, the diameter of the inner hollow circle is 5 mm, and the thickness of the elastomer is 5 mm. It is convenient to install a strain gauge on a flat surface. Therefore, 5 more designs with flat surfaces tangent to the spiral link and different link lengths have been proposed that meet the size requirement of the sensor. Design 1 to Design 5 have stiffness less than 1.69 Nm/rad. Therefore, Design 6 is not fabricated. Design 1 to Design 3 meets the strength requirement. INA125P is used for amplification of the signal from the strain gauge bridge circuit. NI myrio 1900 is used for reading the voltage and averaging filter is used to clean the signal from noise. The results of stress, strain, rotation, and voltage are all linear in response to the torque applied. The sensor meets all the design requirements for the finger exoskeleton.

REFERENCES

[1] Centers for Disease Control and Prevention, "Stroke Facts," *U.S. Department of Health & Human Services*, 2013. http://www.cdc.gov/stroke/facts.htm (accessed Jun. 04, 2021).

[2] R. P. Ubeda, S. C. Gutiérrez Rubert, R. Z. Stanisic, and Á. P. Ivars, "Design and manufacturing of an ultra-low-cost custom torque sensor for robotics," *Sensors (Switzerland)*, vol. 18, no. 6, 2018, doi: 10.3390/s18061786.

[3] Y. Kim, J. Lee, and J. Park, "Compliant joint actuator with dual spiral springs," *IEEE/ASME Trans. Mechatronics*, vol. 18, no. 6, pp. 1839–1844, 2013, doi: 10.1109/TMECH.2013.2260554.

[4] K. Han, L. Chen, M. Xia, Q. Wu, Z. Xu, and G. Wang, "Design and optimization of a high sensitivity joint torque sensor for robot fingers," *Meas. J. Int. Meas. Confed.*, vol. 152, p. 107328, 2020, doi: 10.1016/j.measurement.2019.107328.

[5] Y. Lou, J. Wei, and S. Song, "Design and Optimization of a Joint Torque Sensor for Robot Collision Detection," *IEEE Sens. J.*, vol. 19, no. 16, pp. 6618–6627, 2019, doi: 10.1109/JSEN.2019.2912810.

[6] K. Tandel, H. Patolia, and D. V. Patel, "Design and Analysis of Force/Moment Sensor for a Robot," vol. 1, pp. 60–53, 2018, doi: 10.29007/x5j9.

[7] H. Khan, M. D'Imperio, F. Cannella, D. G. Caldwell, A. Cuschieri, and C. Semini, "Towards scalable strain gauge-based joint torque sensors," *Sensors (Switzerland)*, vol. 17, no. 8, pp. 1–17, 2017, doi: 10.3390/s17081905.

[8] N. Hendrich, F. Wasserfall, and J. Zhang, "3D Printed Low-Cost Force-Torque Sensors," *IEEE Access*, vol. 8, pp. 140569–140585, 2020, doi: 10.1109/ACCESS.2020.3007565.

[9] N. Kashiri, J. Malzahn, and N. G. Tsagarakis, "On the Sensor Design of Torque Controlled Actuators: A Comparison Study of Strain Gauge and

Encoder-Based Principles," *IEEE Robot. Autom. Lett.*, vol. 2, no. 2, pp. 1186–1194, 2017, doi: 10.1109/LRA.2017.2662744.

[10] P. Billeschou, C. Albertsen, J. C. Larsen, and P. Manoonpong, "A Low-Cost, Compact, Sealed, Three-Axis Force/Torque Sensor for Walking Robots," *IEEE Sens. J.*, vol. 21, no. 7, pp. 8916–8926, 2021, doi: 10.1109/JSEN.2021.3049947.

[11] M. T. Ha and C. G. Kang, "Elastic structure for a multi-axis forcetorque sensor," *J. Mech. Sci. Technol.*, vol. 34, no. 1, pp. 23–31, 2020, doi: 10.1007/s12206-019-1203-3.

[12] K. i, B. an, W. peng ao, H. bo eng, Y. li u, and S. guo ang, "Miniature 6-axis force/torque sensor for force feedback in robot-assisted minimally invasive surgery," *J. Cent. South Univ.*, vol. 22, no. 12, pp. 4566–4577, 2015, doi: 10.1007/s11771-015-3007-7.

[13] S. H. Jeong, H. J. Lee, K. R. Kim, and K. S. Kim, "Design of a miniature force sensor based on photointerrupter for robotic hand," *Sensors Actuators, A Phys.*, vol. 269, pp. 444–453, 2018, doi: 10.1016/j.sna.2017.11.052.

[14] Y. Liu, T. Tian, J. Chen, F. Wang, and D. Zhang, "A highly reliable embedded optical torque sensor based on flexure spring," *Appl. Bionics Biomech.*, vol. 2018, 2018, doi: 10.1155/2018/4362749.

[15] H. X. Zhang, Y. J. Ryoo, and K. S. Byun, "Development of torque sensor with high sensitivity for joint of robot manipulator using 4-Bar linkage shape," *Sensors (Switzerland)*, vol. 16, no. 7, 2016, doi: 10.3390/s16070991.

[16] G. Palli and S. Pirozzi, "An Optical Torque Sensor for Robotic Applications," *Int. J. Optomechatronics*, vol. 7, no. 4, pp. 263–282, 2013, doi: 10.1080/15599612.2013.879500.

[17] X. Sun *et al.*, "Design of a large-range torque sensor with variable resolutions," *Meas. J. Int. Meas. Confed.*, vol. 174, no. December 2020, p. 109032, 2021, doi: 10.1016/j.measurement.2021.109032.

[18] L. Fu, A. Song, and D. Chen, "A Polyetheretherketone Six-Axis Force/Torque Sensor," *IEEE Access*, vol. 7, pp. 105391–105401, 2019, doi: 10.1109/ACCESS.2019.2932387.

[19] S. Hu, H. Wang, Y. Wang, and Z. Liu, "Design of a novel six-axis wrist force sensor," *Sensors (Switzerland)*, vol. 18, no. 9, 2018, doi: 10.3390/s18093120.

[20] Y. B. Kim, U. Kim, D. Y. Seok, J. So, and H. R. Choi, "A novel capacitive type torque sensor for robotic applications," in *IEEE/ASME International Conference on Advanced Intelligent Mechatronics, AIM*, 2016, vol. 2016-Septe, pp. 993–998, doi: 10.1109/AIM.2016.7576899.

[21] F. Aghili, M. Buehler, and J. M. Hollerbach, "Design of a hollow hexaform torque sensor for robot joints," *Int. J. Rob. Res.*, vol. 20, no. 12, pp. 967–976, 2001, doi: 10.1177/02783640122068227.

[22] "ASM Material Data Sheet," *Matweb*. http://asm.matweb.com/search/SpecificMaterial.asp?bassnum=MA2024T4 (accessed Jan. 09, 2021).

[23] "ASM Material Data Sheet," *Matweb*. http://asm.matweb.com/search/SpecificMaterial.asp?bassnum=MA2024T4 (accessed Jan. 09, 2021).

[24] "ASM Material Data Sheet," *Matweb*. http://asm.matweb.com/search/SpecificMaterial.asp?bassnum=MA2024T4 (accessed Jan. 19, 2021).

[25] S. When *et al.*, "Comparison of typical 3D printing materials," *iGEM*, 2016. http://2015.igem.org/wiki/images/2/24/CamJIC-Specs-Strength.pdf (accessed Jan. 09, 2021).

[26] Cambridge University Engineering Department, "Material Data Book," 2003. http://www-mdp.eng.cam.ac.uk/web/library/enginfo/cueddatabooks/materials.pdf (accessed Jan. 01, 2021).

[27] W. Zhang *et al.*, "Design and Characterization of a Novel T-Shaped

Multi-Axis Piezoresistive Force/Moment Sensor," *IEEE Sens. J.*, vol. 16, no. 11, pp. 4198–4210, Jun. 2016, doi: 10.1109/JSEN.2016.2538642.

[28] Y. Park *et al.*, "Exoskeletal Force-Sensing End-Effectors With Embedded Optical Fiber-Bragg-Grating Sensors," *IEEE Trans. Robot.*, vol. 25, no. 6, pp. 1319–1331, 2009.

[29] J. Ma and A. Song, "Fast estimation of strains for cross-beams six-axis force/torque sensors by mechanical modeling," *Sensors (Switzerland)*, vol. 13, no. 5, pp. 6669–6686, 2013, doi: 10.3390/s130506669.

[30] OMEGA, "Pre-Wired Strain Gages," *Omega Engineering Inc.*, 2014. http://www.omega.com/pptst/KFH.html (accessed Jan. 01, 2021).

[31] "DY Strain Gauges with 2 Parallel Measuring Grids for Measurements on Bending Beams," *HBM*. https://www.hbm.com/en/3427/dy-double-strain-gauges-with-1-measurement-grid/ (accessed Jan. 21, 2021).

[32] "HAPTICA." http://www.hapticasensing.com/wp-content/uploads/2020/05/Table_Products_Backed_Single_Gauges_2005.pdf (accessed Jan. 21, 2021).

[33] "KFGS Series General-purpose Foil Strain Gages," *Kyowa*. https://www.kyowa-ei.com/eng/product/category/strain_gages/kfgs/index.html (accessed Jan. 21, 2021).

[34] E. Cakit, B. Durgun, O. Cetik, and O. Yoldas, "A survey of hand anthropometry and biomechanical measurements of dentistry students in Turkey," *Hum. Factors Ergon. Manuf.*, vol. 24, no. 6, pp. 739–753, 2014, doi: 10.1002/hfm.20401.

[35] S. Ueki *et al.*, "Development of a Hand-Assist Robot With," *IEEE/ASME Trans. MECHATRONICS*, vol. 17, no. 1, pp. 136–146, 2012.

[36] A. Baldoni, M. Cempini, M. Cortese, S. Crea, M. C. Carrozza, and N. Vitiello, "Design and validation of a miniaturized SEA transmission system," *Mechatronics*, vol. 49, no. December 2017, pp. 149–156, 2018, doi: 10.1016/j.mechatronics.2017.12.003.

[37] “INA125P Datasheet - Texas Instruments,” *Texas Instruments*. https://www.alldatasheet.com/datasheet-pdf/pdf/847623/TI1/INA125P.html.